

REPORTE TÉCNICO
**Reconocimiento
de Patrones**

**Iris Segmentation Methods and
Current Challenges: State of the Art**

**Yasiel Sánchez González, José Luis Gil
Rodríguez y Eduardo Garea Llano**

RT_059

enero 2014





CENATAV

Centro de Aplicaciones de
Tecnologías de Avanzada
MINISTERIO DE LA INDUSTRIA BÁSICA

RNPS No. 2142
ISSN 2072-6287
Versión Digital

SERIE AZUL

REPORTE TÉCNICO
**Reconocimiento
de Patrones**

**Iris Segmentation Methods and
Current Challenges: State of the Art**

**Yasiel Sánchez González, José Luis Gil
Rodríguez y Eduardo Garea Llano**

RT_059

enero 2014



Table of Content

1	Introduction	2
2	Iris texture segmentation.....	3
2.1	Integro-differential operator.....	5
2.2	Hough's transform.....	7
2.2.1	Methods based on Hough's transformation	8
2.3	Iterative methods for Iris segmentation.....	9
2.4	Method based on Active Contours.....	10
2.4.1	Other methods based on Active Contours	13
2.4.2	Geodesic Active Contours approach	14
2.5	Combining strategies for iris inner and outer border localization	17
2.6	Other Iris segmentation methods	21
3	Segmentation of noisy Iris images methods	22
4	Discussion and challenging about iris segmentation	25
4.1	Iris images databases.....	25
4.1.1	CASIA-Iris	26
4.1.2	ICE	28
4.1.3	MMU.....	28
4.1.4	ND.....	28
4.1.5	UBIRIS.....	29
4.1.6	WVU-Biomdata	29
4.1.7	Other public databases	30
4.2	Comparison of existing methods.....	31
4.3	Challenges in Iris segmentation	33
5	Conclusion.....	36
	References.....	36

Iris Segmentation Methods and Current Challenges: State of the Art

Yasiel Sánchez González, José Luis Gil Rodríguez y Eduardo Garea Llano

Pattern Recognition Department, Advanced Technology Application Center (CENATAV),
La Havana, Cuba
{ysanchez, jlgil, egarea}@cenatav.co.cu

RT_059, Serie Azul, CENATAV
Aceptado: 12 de diciembre de 2013

Abstract. Under ideal image acquisition, iris biometric data provide high performance of people recognition compared with other biometric features. However, the overall performance of such systems can be reduced by non-ideal conditions, such as in unconstrained, on-the-move, covert, or non-collaborative setups. In particular, a critical step in the recognition process is the segmentation of the iris pattern in the input image of the eye. The eyelids, eyelashes and reflections are iris pattern occlusions that can cause errors in the segmentation process. As a result, incorrect segmentation can cause erroneous biometric recognition and seriously reduces the final accuracy of the system. For this reason, in this report we review the main research developed for iris texture segmentation and its progress in the last years, we also discuss the most recent results as well as the challenges associated with the iris segmentation process. Furthermore, we analyze methods used to refine and eliminate noise (reflections, occlusions, etc.), causing difficulties in the segmentation process. In general, the aim of this paper is to provide an overview of the progress made in iris segmentation.

Keywords: iris segmentation methods, segmentation methods of noisy iris images, challenges in iris segmentation, iris biometric.

Resumen. En condiciones ideales de adquisición de imágenes, los datos biométricos del iris proporcionan un alto rendimiento en el reconocimiento de personas en comparación a otros rasgos biométricos. Sin embargo, el desempeño global de estos sistemas se puede reducir en condiciones no ideales, tales como condiciones no controladas, en condiciones de movimiento, o no colaborativas. En particular, un paso crítico del proceso de reconocimiento es la segmentación del patrón del iris en la imagen de entrada del ojo. Los párpados, las pestañas y las reflexiones son oclusiones del patrón del iris que pueden causar errores en el proceso de segmentación. Como resultado, una segmentación incorrecta puede producir reconocimientos biométricos erróneos y reducir seriamente la precisión final del sistema. Por esta razón en este reporte se revisan las principales investigaciones desarrolladas para la segmentación de la textura del iris y su avance en los últimos años. Además se discute sobre los resultados más recientes así como los retos asociados al proceso de segmentación del iris. Por otra parte, se presentan métodos para refinar y eliminar los ruidos (reflexiones, oclusiones, etc.) que dificultan esta tarea, y se ofrece una visión general de los progresos realizados en la segmentación del iris.

Palabras clave: métodos de segmentación del iris, métodos de segmentación de imágenes de iris ruidosas, retos en segmentación de iris, biometría de iris.

1 Introduction

Nowadays, due to technological advances and the increasing demand for security systems and video surveillance, biometric applications have taken a great importance [1]. Biometrics is the discipline that identifies individuals based on their physical characteristics and/or behavior. The main physical characteristics are fingerprints, iris, retina, hand geometry and facial features. Moreover, within the most common behavioral characteristics include signature, gait, voice and keyboard-click.

Biometric systems are used in two main tasks: verification and identification. Verification is a process of recognizing one to one (1: 1), based on the comparison of two biometric samples. It is an explicit form of authentication, as is generally known in computer science, where it comes to determining whether a person is who he claims to be or not. While the identification, is the recognition of a biometric sample in a set of previously stored samples n (1: n). This task aims to identify a person from a group of individuals. Below, some current examples of biometric applications systems are listed [2]:

- ❖ Banking,
- ❖ Financial and commercial,
- ❖ Access to premises and facilities,
- ❖ Access to computers and computer networks,
- ❖ Immigration and Travelling,
- ❖ E-commerce and telephony services,
- ❖ Security in prisons,
- ❖ Identification of people

Each biometric feature, either physical or behavioral, is different and there are several factors that determine their suitability for use in a biometric system. Table 1 shows a comparison of the behavior of some of these factors in the different biometric techniques [3].

Table 1. Comparison of various biometric techniques. [3]

	Iris	Fingerprint	Voice	Hand geometry	Face
Reliability	Very high	High	High	High	High
Ease of Use	Medium	High	High	High	High
Security against attacks	Very high	High	Medium	High	Medium
Acceptance	Medium	Medium	High	High	Very high
Stability	High	High	Medium	High	Medium

The recognition of individuals by the texture of the iris, is one of the main biometric methods. It has a high reliability, stability and high security against attacks.

The iris begins its development during the third month of gestation [4] and the structures that determine the pattern are fully formed at eight months [5]. The final appearance of the iris is not reached up to the first year of life and from this point will remain almost constant. The iris texture complexity in both eyes are the most distinctive features where many biometric data can be used, see (Fig 1). The iris contains some small details that are unique to each individual. Even twins don't have the same iris patterns [6]. This uniqueness and permanence of iris patterns makes these biometrics popular and robust.

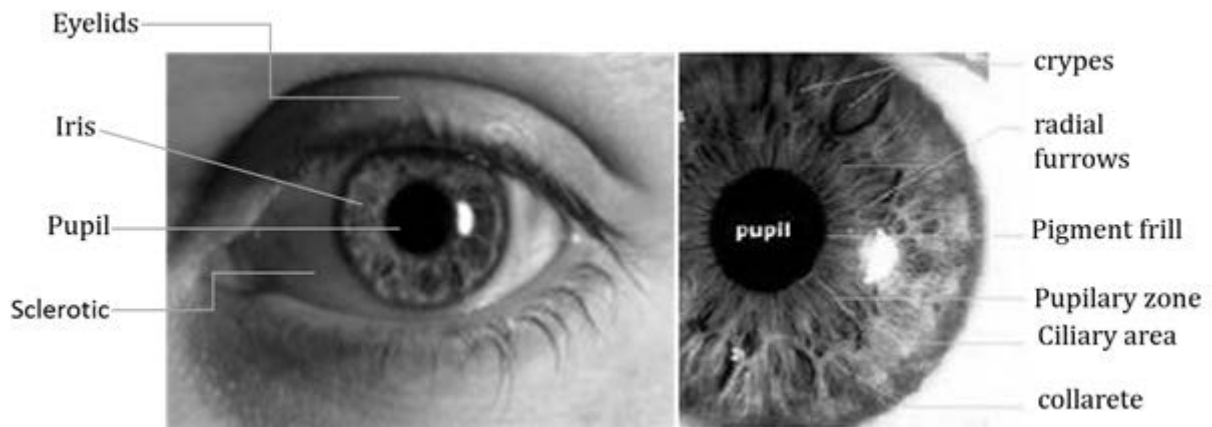


Fig. 1. Human eye, characteristics of the iris and anatomy of the eye.

As it was mentioned above, the iris recognition is one of the most reliable biometric methods nowadays; studies have demonstrated dependability 1 in 16 million find two exactly equal iris, as a result, has a high recognition accuracy.

One of the major issues in the development of iris recognition systems is the decreasing performance of such systems in non-ideal contexts, such as in unconstrained, on-the-move, covert, or non-collaborative setups. In particular, a critical step of the biometric recognition process is related to the ability of the image processing system to effectively locate and separate the iris pattern in the input face/eye image. This process, referred as iris segmentation, still presents many challenges. The iris region, in fact, is a small moving area, and it is often occluded by eyelids and eyelashes. These problems are especially relevant when the user does not face the camera or is walking from a considerable distance. Moreover, the correct detection of the iris boundaries and the removal of the occlusions are directly related to the accuracy of the iris recognition system.

Novel approaches and currently research trends in the detection of the iris region aim to achieve a more robust and accurate localization of the iris pattern even in non-ideal conditions, in order to allow the application of iris recognition systems in a broader range of scenarios. Similarly, the ability to correctly segment and enhance the iris images captured even from a great distance could result in an even higher control over critical transit points.

In this report, we study the main and new methods used for iris segmentation. In Section 2 the classical methods, integro-differential operator and circular Hough transform, are reviewed. Then, a description of other prominent approaches is presented, like iterative methods, based on active contours and methods that perform segmentation by combined strategies. Some methods, which do not fall in any specific category, are also described, followed by a survey of the methods for the detection of occlusions and reflections. Finally, the recent actions in iris segmentation methods and challenges in this field are discussed.

2 Iris texture segmentation

The iris recognition process is relatively complex and involves several stages of processing as is illustrated in (Fig. 2). The four basic stages that compose an iris recognition system are: “image acquisition”, “image segmentation”, “analysis and representation of the iris features”, and “matching of iris representations” [7].

The image acquisition stage is usually composed by cameras that capture images in the near-infrared range (700 – 900nm). The ISO Iris Image Standard requires that the length of the iris diameter is at least 200 pixels [8]. The user cooperation is usually required in order to properly capture the iris image.

The image segmentation stage performs the localization of the iris in the image and removes the areas corresponding to eyelids, eyelashes, reflections, and shadows [9]. Typically, the iris segmentation is the most time-consuming step [10] and its effectiveness is relevant because the obtained accuracy strongly influences the results of the biometric system [11]. An incorrectly segmented iris, in fact, can result into errors of the matching module.

The feature extraction stage is based on algorithms that analyze the segmented iris image and extract the distinctive features from the iris texture pattern. Then these extracted features are used to compute an abstract representation, called template. One of the most commonly used templates is the IrisCode [12].

The last stage computes a matching distance between two or more templates, in order to determine if they belong to the same person. In most of the cases, the matching value is computed as the Hamming Distance between shifted templates [12], [13]. Other distances like Levenshtein distance [14] and Euclidean distance [15] have been used by researchers.

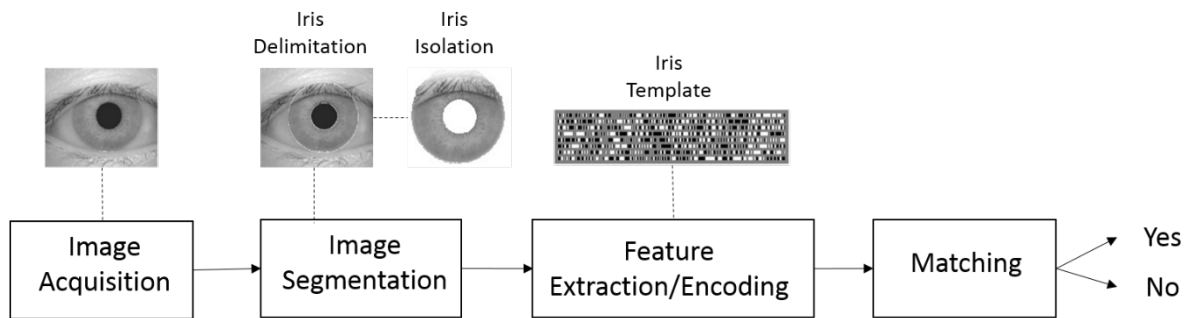


Fig. 2. Processing stages of an iris recognition system.

A critical step of the recognition process is the segmentation of the iris texture in the input face/eye image. This process has to deal with the fact that the iris region of the eye is relatively a small area, wet and constantly in motion due to involuntary eye movements. Besides, eyelids, eyelashes and reflections are occlusions of the iris texture that can cause errors in the segmentation process. As a result, an incorrect segmentation can produce erroneous biometric recognitions and seriously reduce the final accuracy of the system.

The iris segmentation methods are oriented toward isolating the iris of an image. This is usually performed in two steps: first the inner and outer boundaries of the iris region are estimated, then the occlusions and reflections are detected and removed. Both, the inner boundary and the outer boundary of a typical iris can approximately be taken as circles. However, the two circles are usually not concentric [15] [16]. Their correct delimitation is an important requirement. Fig. 3 shows a taxonomy that organizes the existed methods to carry out iris segmentation images.

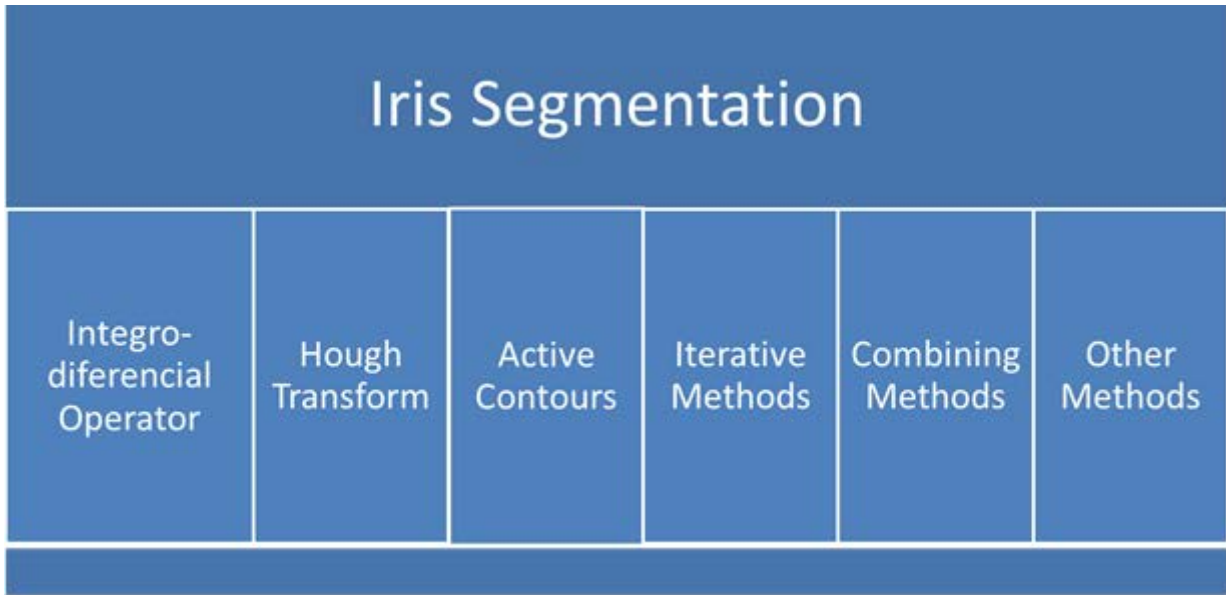


Fig. 3. Proposed taxonomy of the iris segmentation methods.

The following table briefly describes most of the methods analyzed in the proposed taxonomy.

Table 2. Brief description of the iris segmentation methods included in the proposed taxonomy.

Methods	Brief description	References
Integro-diferencial Operator	This operator serves as a circle finder which searches the maximum angular integral of radial derivative over the image domain. Locates the iris inner and iris outer border with an integro - differential operator.	[2]
Wildes approach	Use the Hough Transform in order to locate the inner and outer iris border.	[17]
Active Contours	Locate the iris within an image, modeling the iris as a non-concentric partial rings.	[18]
Iterative Methods	Iterative methods, as the name suggests, are based on running a few rounds to converge to the solution. These methods begin by selecting a random starting point to find the region of interest, from this point begins to iterate and to better estimate more refined iris boundaries using techniques such as neural networks, Fourier spectral density, etc.	[19],[20],[21],[22],[23]
Combining strategies	The hybrid and incremental methods combine techniques from different classes, performing the iris segmentation in an incremental way.	[24],[25],[26], [27]

2.1 Integro-differential operator

This technique was first proposed in [2], and is one of the most used segmentation methods in the literature. The first step consists in the estimation of two circumferences that approximate the inner and outer iris boundaries. Then, the upper and lower eyelid boundaries are searched and approximated by

two curves. The estimation of the circumferences that describe the inner and outer boundaries of the iris is performed by an algorithm that iteratively tests different possible center coordinates and radius values. The result of this algorithm is the circumference corresponding to a greater value resulting from the application of an integro-differential operator. The used integro-differential operator is defined as: (Fig. 4).

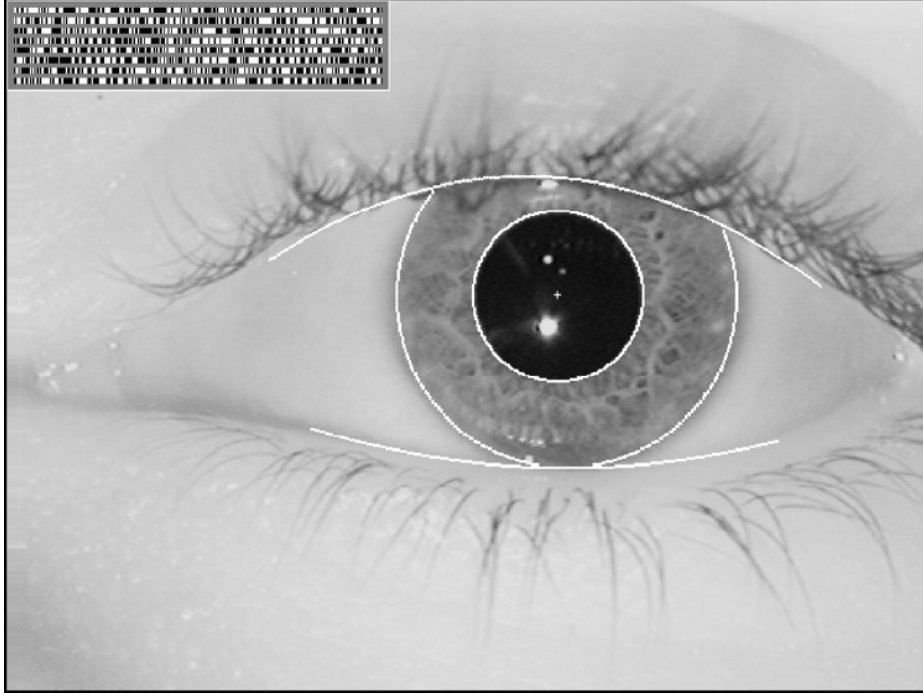


Fig. 4. Localizing the iris boundaries by Integro-differential operator. [2]

The equation is as follows:

$$\max_{(r, x_0, y_0)} \left| G_\sigma(r) * \frac{\alpha}{\alpha_r} \int_{(r, x_0, y_0)} \frac{I(x, y)}{2\pi r} ds \right|, \quad (1)$$

where: $I(x, y)$ is an image containing an eye. The operator searches over the image domain (x, y) for the maximum in the blurred partial derivative with respect to increasing radius r , of the normalized contour integral of $I(x, y)$ along a circular arc ds of radius r and center coordinates (x_0, y_0) . The symbol $*$ denotes convolution and $G_\sigma(r)$ is a smoothing function such as a Gaussian of scale σ . The complete operator behaves as a circular edge detector, blurred at a scale set by σ , searching iteratively for the maximal contour integral derivative at successively finer scales of analysis through the three parameters space of center coordinates and radius (x_0, y_0, r) defining a path of contour integration.

The integro-differential operator provides a fast and accurate detection of both boundaries of the iris when the image is acquired under ideal conditions. However, it may fail to detect when there is noise in the eye images, such as reflections, since it works only locally. In literature, there are many variants of this method, which seek to improve these problems. For example, there are algorithms designed to reduce the required computational time [28];[29], or to improve the segmentation accuracy [30]; [31]. Xinying et al., improves the accuracy of the algorithm in two aspects. The first one, initially they locate the iris by a fast coarse approach and after that apply a finer localization. The second one was designed to exclude the iris area that can be covered by the eyelids and eyelashes. Moreover, in [29] proposed to

improve the Daugman's method by solving the problem of the location of potential centers, taking an Average Square Shrinking (ASS) approach to locate the potential primary centers. It also focus on circle sampling (CS) to evaluate how many points should be accessed on circle contour for computing Daugman's integral. It also corresponds to the angle of division circle around the contour. High value for CS clearly reduces the estimation error of Daugman's integral compute. This makes the method run with less computational time.

2.2 Hough's transform

Another important technique used for the estimation of the iris boundaries is based on the Hough transform. Hough transform is a standard image analysis tool for finding curves that can be defined in a parametrical form such as lines, polynomials and circles. The recognition of a global pattern is achieved using the local patterns. For instance, recognition of a circle can be achieved by considering the strong edges in an image as the local patterns and searching for the maximum value of a circular Hough transform.

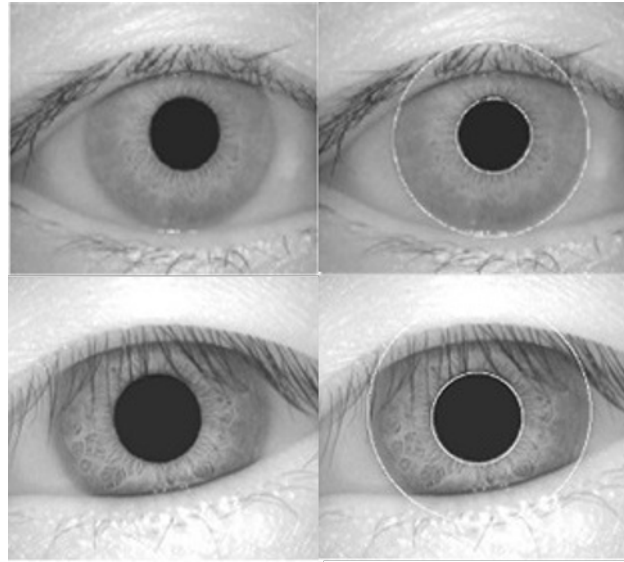


Fig. 5. Segmentation by Hough's Transform.

Many authors use the Hough transform such as [32]; [33]; [17]. In the proposed method by [17], an edge map of the image is first obtained by thresholding the magnitude of the image intensity gradient:

$$|\nabla G_{(x,y)} * I(x,y)|, \quad (2)$$

where $\nabla \equiv (\partial/\partial_x, \partial/\partial_y)$ and $G_{(x,y)} = \frac{1}{2\pi\sigma^2} e^{-\frac{(x-x_0)^2 + (y-y_0)^2}{2\sigma^2}}$. $G_{(x,y)}$ is a Gaussian smoothing function with scaling parameter $\frac{3}{4}$ to select the proper scale of edge analysis.

The edge map is then used in a voting process to maximize the defined Hough transform for the desired contour. Considering the obtained edge points as (x_j, y_j) , $j = 1, 2, 3, \dots, n$, a Hough transform can be written as:

$$H(x_c, y_c, r) = \sum_{j=1}^n h(x_j, y_j, x_c, y_c, r), \quad (3)$$

where

$$H(x_j, y_j, x_c, y_c, r) = \begin{cases} 0 & \text{otherwise} \\ 1 & \text{if } g(x_j, y_j, x_c, y_c, r) = 0. \end{cases}$$

The limbus and pupil are both modeled as circles and the parametric function g is defined as:

$$g(x_j, y_j, x_c, y_c, r) = (x_j - x_c)^2 + (y_j - y_c)^2 - r^2. \quad (4)$$

Assuming a circle with a center (x_c, y_c) and a radius r , the edge points that are located over the circle result in a zero value of the function. The value of g is then transformed to 1 by the h function, which represents the local pattern of the contour. The local patterns are then used in a voting procedure using the Hough transform, H , in order to locate the proper pupil and limbus boundaries. In order to detect limbus, only vertical edge information is used. The upper and lower parts, which have the horizontal edge information, are usually covered by the two eyelids. The horizontal edge information is used for detecting the upper and lower eyelids, which are modeled as parabolic arcs.

2.2.1 Methods based on Hough's transformation

In literature, there are many different iris segmentation methods based on the Hough transform, the main difference consists in the algorithms used for the estimation of the edges. The choice of these algorithms is related to the applicative context. In [16] it is proposed a modified version of the Hough Transform based on Texture Segmentation, selecting randomly three edge points in the edge map and computing the centroid and radius according to the Eq. (5).

The method proposed in [34] first, employ Integral Projection Functions to estimate the pupil center and then the estimation of the radius of the pupil. A weight ring mask which embraces the pupil edge is created. The last step is to use the weighted Hough transform to extract the final precise pupil center and radius.

A well-known fuzzy-clustering algorithm is used in [35] for extracting three discrete values for each pixel of the image, labeling (classifying) each pixel. Subsequently, it is employed a Canny edge detector and used as input to apply the Hough transform. In (Fig 6) the block diagram of this segmentation algorithm is shown.

$$(x_i - a)^2 + (y_i - b)^2 = r^2. \quad (5)$$

In [36], the author implemented open-source Wildes segmentation method. He used Canny edge detection to detect iris edge points. First, vertical edges are used to detect the outer iris boundary and then horizontal edges to detect inner iris boundary. To separate eyelids from the iris, a horizontal line obtained after a linear Hough transform application on the image isolates each eyelid from the iris. Eyelashes and specular reflections are segmented by an intensity threshold. This software is used as a reference method in many scientific publications.

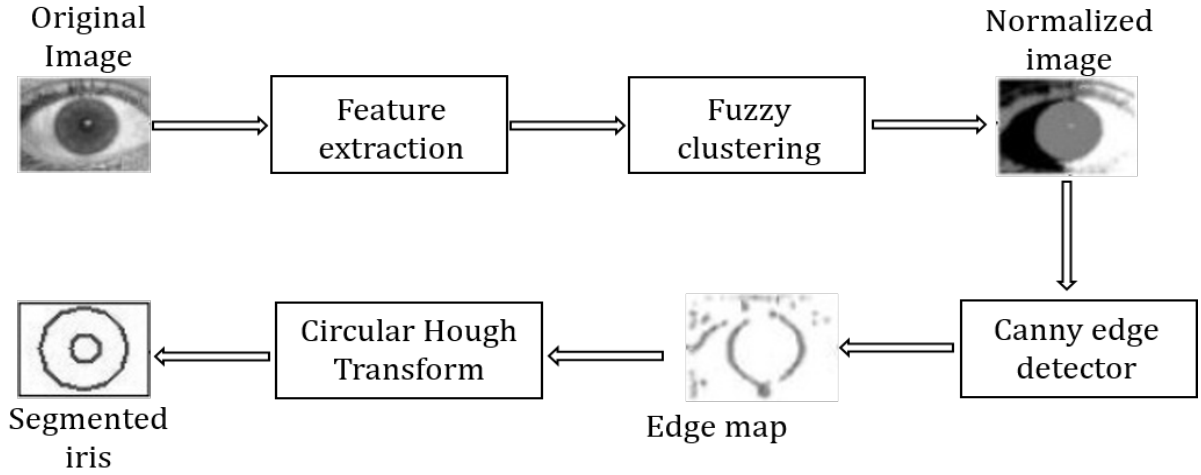


Fig. 6. Block diagram of the proposed methodology by [35].

[37] proposes a localization algorithm with dual coarse-to-fine strategy for both iris boundaries (inner and outer). In the coarse stage, the lower contour of the pupil is used to estimate the parameters of the inner boundary, while the average intensity signals on both sides of the pupil are used to estimate the parameters of the outer boundary. In the final stage, the Hough transform is used to obtain the precise parameters with the gradient information. There are also methods based on the Hough transform and designed in order to obtain good performances in terms of computational time [38];[39].

One can say that the Hough Transform as integro-differential operator is one of the most used techniques, only changes the way of estimating the edges. Hough Transform presents a number of problems. First of all, it requires threshold values to be chosen for edge detection, and this may result in critical edge points being removed, resulting in failure to detect circles/arcs. Secondly, the Hough's transform is computationally intensive due to its "brute-force" approach, and thus, it may not be suitable for real time applications.

2.3 Iterative methods for Iris segmentation

In literature, there are also iterative methods for estimation of iris boundaries. The method proposed by [19] is initialized with a circle in the center of the pupil, choosing the radius of the circle slightly larger than that of the pupil in order to apply a force on selected points of the circle. The magnitude and the direction of the force are determined by two properties of the iris and its outer boundary (a) the iris is (on average) darker than the sclera, (b) the transition from dark to light is steepest on the exact location of the boundary. Once the force has been applied to all points, a new location for the center of the iris is estimated. The equation of a circle is used as a starting point in building a linear estimation model:

$$x_i^2 + y_i^2 = r^2 - x^2 - y^2 + 2x_ix_c + 2y_iy_c . \quad (6)$$

The radius is estimated by finding an estimate \hat{r} that minimizes the mean square error distance between the boundary of the circle and the N points. It is simply the mean distance from the estimated center to the measured boundary points:

$$\hat{r} = \frac{1}{N} \sum_{i=1}^N \sqrt{(\hat{x}_i - x_i)^2 + (\hat{y}_i - y_i)^2} . \quad (7)$$

The solution is obtained when both the center and the radius are less than one pixel.

The method proposed in [20] is an iterative algorithm, which starts at a random point in the input image, pretending to locate the center of the pupil through the iterative refinement of the current image. This method is able to locate the local properties in the current image, estimating the x and y towards the center of the pupil. Each iteration of the proposed method consists of two stages (a) a local estimation of a set of image characteristics and (b) an estimation of the pupil center position with two artificial neural networks.

[21] developed an iterative algorithm to locate with precision the limits of limbus and eyelids. In each iteration this algorithm seeks limits excluding eyelid areas identified for the next iteration, to detect the boundaries using the method proposed by [12].

The method presented in [40] performs an iterative search of the circumferences that approximate the inner and outer iris boundaries by maximizing the function:

$$D = \sum_m \left(\sum_{k=1}^5 (I_{n,m} - I_{n-k,m}) \right), \quad (8)$$

where $I_{i,j} = I(x_0 + i\Delta_r \cos(j\Delta_\theta), y_0 + i\Delta_r \sin(j\Delta_\theta))$, $I(x, y)$ is the image intensity, Δ_θ is the angle increment and Δ_r is the radius increment.

The method presented in [22] first estimates the inner iris boundary and then estimates the outer boundary by using an iterative approach. The area of the image used to search the center of the circumference approximating the outer boundary is limited to the pixels that are close to the pupil center. The approximated circumference is defined as a weighted circular integral of local signal to noise ratio (SNR) values:

$$\max_{(x_c, y_c, r)} \oint_{(x_c, y_c, r)} w_{x_c, y_c} \frac{SNR(x, y)}{2\pi r} ds, \quad (9)$$

where $SNR(x, y)$ is the ratio of the local mean to the local standard deviation at the position (x, y) , and w_i is a weight value, define as $w_i = 1 - (d_i/d_{max})$.

A well-known iris recognition system is proposed in [23]. This system approximates the inner and outer iris boundaries by two circumferences. The first step consists in the localization of the pupil center by using an edge detection technique. Then, the inner and outer iris boundaries are estimated as two concentric circumferences. The radii are estimated by considering the limits described by the edges. The method proposed in [41] binarizes the image by using the information related to the Fourier spectral density and then estimates the circumferences that describe the inner and outer iris boundaries by using a geometrical approach.

2.4 Method based on Active Contours

Algorithms based on active contours, or snakes, iteratively adapt the segmented shape to the edges of the image. This class of algorithms is commonly adopted in many computer vision applications.

Ritter [18] proposed the first active contour model to localize the iris in an image. The model detects pupil and limbus by activating and controlling the active contour using two defined forces: internal and external forces. The internal forces are responsible to expand the contour into a perfect polygon with a radius δ larger than the contour average radius. The internal force, $F_{int,i}$, applied to each vertex, V_i , is defined as:

$$F_{int,i} = \bar{V}_i - V_i, \quad (10)$$

where \bar{V}_i is the position of this vertex in the perfect polygon. The position of \bar{V}_i can be obtained with respect to C_r , the average radius of the current contour, and the contour center, $C = (C_x, C_y)$. The center of a contour is defined as:

$$C = (X_c, Y_c) = \frac{1}{n} \sum_{i=1}^n V_i, \quad (11)$$

which is the average position of all contour vertices. The average radius of the contour is defined as:

$$C_r = \frac{1}{n} \sum_{i=1}^n \|V_i - C\|, \quad (12)$$

which is the average distance of all the vertices from the defined center point. The position of the vertices of the expected perfect polygon is then obtained as:

$$\bar{V}_i = (C_x + (C_r + \delta) \cos(2\pi i/n), C_y + (C_r + \delta) \sin(2\pi i/n)), \quad (13)$$

where n is the total number of vertices.

The internal forces, (Fig.7), are designed to expand the contour and keep it circular. The force model assumes that pupil and limbus are globally circular, rather than locally, to minimize the undesired deformations due to specular reflections and dark patches near the pupil boundary.

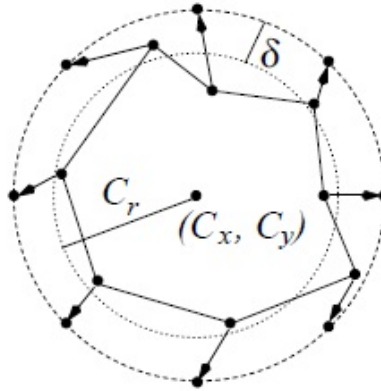


Fig. 7. The internal forces of the Discrete Circular Active Contour. [18]

The contour detection process of the model is based on the equilibrium of the defined internal forces with the external forces. The external forces are obtained from the grey level intensity values of the image and are designed to push the vertices inward. The magnitude of the external forces is defined as:

$$\| F_{ext,i} \| = I(V_i) - I(V_i + \hat{F}_{ext,i}), \quad (14)$$

where $I(V_i)$ is the grey level value of the nearest neighbor to V_i . $\hat{F}_{ext,i}$ is the direction of the external force for each vertex and it is defined as a unit vector given by:

$$\hat{F}_{ext,i} = \frac{C - V_i}{\|C - V_i\|}. \quad (15)$$

Therefore, the external force over each vertex can be written as:

$$F_{ext,i} = \| F_{ext,i} \| \hat{F}_{ext,i}. \quad (16)$$

The movement of the contour is based on the composition of the internal and external forces over the contour vertices. Replacement of each vertex is obtained iteratively by:

$$V_i(t + 1) = V_i(t) + \beta F_{int,i} + (1 - \beta) F_{ext,i}, \quad (17)$$

where β is a defined weight that controls the phase of the contour movement and sets the equilibrium condition of internal and external forces. The final equilibrium is achieved when the average radius and center of the contour becomes the same as the one in m iterations ago.

The pseudo-code below shows the search process for iris edges [18].

Algorithm: Find Iris Border

```

Initialise  $\delta$ ,  $\delta_\epsilon$ ,  $\delta_{\epsilon 0}$ ,  $\delta_{last1}$ , and  $\delta_{last2}$ 
Initialise bounceError to false
WHILE  $\delta$  lies between  $\delta_{min}$  and  $\delta_{max}$ 
    AND bounceError is false
    AND the contour is not in equilibrium
    Initialise the contour
    WHILE the contour is not in equilibrium
        AND the contour is in the image
        AND the contour is not too large
        AND the contour is not too small
        AND not maxIterations
        Move the contour points using (17)
    ENDWHILE
    IF the contour is too large
        OR the contour is off the image
        Reduce  $\delta$  by  $\delta_\epsilon$ 
    ELSE IF the contour is too small
        OR maxIterations was reached
        Increase  $\delta$  by  $\delta_\epsilon$ 

```

```

ENDIF
IF equilibrium was not reached
     $\delta_{last2} = \delta_{last1}$ 
     $\delta_{last1} = \delta$ 
    IF  $\delta_{last2} == \delta$  [we have oscillation]
         $\delta_\epsilon = \delta_\epsilon / 10$  [try a smaller change in  $\delta$ ]
    ENDIF
    IF  $\delta_\epsilon < \delta_{\epsilon min}$  [the oscillation cannot be stopped]
        bounceError = true
    ENDIF
ENDIF
ENDWHILE

```

2.4.1 Other methods based on Active Contours

Other method have been proposed by[42]. The author presented a different model of active contours, which is not based on the gradient of the image to the stopping criterion. The energy function is defined as:

$$\begin{aligned}
 F(c_1, c_2, C) = & \int_{inside(C)} |u_0(x, y) - c_1|^2 dx dy \\
 & + \int_{outside(C)} |u_0(x, y) - c_2|^2 dx dy,
 \end{aligned} \tag{18}$$

where u_0 is the image, C is the variable that defines the limits of the contour and the constants c_1 and c_2 are the mean values of the internal and external regions of C , respectively.

In [43], a semantic iris contour map combining spatial information on iris location (obtained by a circular Hough transform) and gradient map as edge indicator is used for level set active contour segmentation. The semantic iris contour map is claimed to reduce the local extremes in iris region misleading the evolution of the iris contour. Tests were performed on ICE (2005) database and CASIA V3 database, reporting efficient and effective results.

In [44] it was proposed two-stage iris segmentation algorithm in which they first estimate the inner and outer boundaries of the iris using an elliptical model. In the second stage, they applied the modified energy function in a narrow band over the estimated boundaries to compute the exact inner and outer boundaries of the iris. The model of the energy function is as follows:

$$\begin{aligned}
 Energy(c) = & \alpha \int_{\Omega} \left\| \frac{\partial \bar{C}}{\partial c} \right\| \phi dc + \beta \iint_{in(C)} |I(x, y) - c_1|^2 dx dy \\
 & + \lambda \iint_{out(C)} |I(x, y) - c_2|^2 dx dy,
 \end{aligned} \tag{19}$$

where \bar{C} is the evolution curve such that $\bar{C} = \{(x, y) : \bar{\psi}(x, y) = 0\}$, c is the curve parameter, \emptyset is the weighting function or the stopping term, Ω represents the image domain, $I(x, y)$ is the original iris image, c_1 and c_2 are the average values of pixels inside and outside \bar{C} , respectively, and α , β and λ are positive constants such that $\alpha < \beta \leq \lambda$. Parameterizing Eq. (19) and deducing the associated Euler-Lagrange equation lead to the following active contour model:

$$\bar{\psi}'_t = \alpha \emptyset(\bar{v} + \epsilon_k) |\nabla \bar{\psi}| + \nabla \emptyset \nabla + \beta \delta(I - c_1)^2 + \lambda \delta \bar{\psi} (I - c_2)^2, \quad (20)$$

where \bar{v} is the advection term, ϵ_k is the curvature-based smoothing term, ∇ is the gradient operator, and $\delta = 0.5/(\pi(x^2 + 0.25))$.

[Daugman, 2007] proposed an Active Contours based approach on the description of the iris boundaries (inner and outer) in term of Fourier series expansions. The estimation procedure is oriented to compute a Fourier expansion of the N regularly spaced angular samples from radial gradient edge data $\{r_\theta\}$ for $\theta = 0$ and $\theta = N - 1$. A set of M discrete Fourier coefficients $\{C_k\}$ for $k = 0$ and $k = M - 1$, are computed from the data sequence $\{r_\theta\}$:

$$C_k = \sum_{\theta=0}^{N-1} r_\theta e^{-2\pi i k \theta / N}; \quad R_\theta = \frac{1}{N} \sum_{k=0}^{M-1} C_k e^{2\pi i k \theta / N}. \quad (21)$$

From these M discrete Fourier coefficients, an approximation to the corresponding iris boundary (now without interruptions and at a resolution determined by M) is obtained as the new sequence $\{R_\theta\}$ for $\theta = 0$ and $\theta = N - 1$, as expressed in Eq.(21).

Off-axis detection and correction is executed by assuming the orthographic image of the iris to reveal a circular pupil, i.e. gaze direction θ and magnitude γ are computed from the boundary as an oriented ellipse:

$$X(t) = a \cos(t) + b \sin(t), Y(t) = c \cos(t) + d \sin(t), \quad (22)$$

where $a = A \cos^2(\theta) + B \sin^2(\theta)$, $b = c = (B - A) \cos(\theta) \sin(\theta)$, and $d = B \cos^2(\theta) + A \sin^2(\theta)$, i.e. parameters a, b, c, d are real and imaginary parts of the complex Fourier coefficients of the empirical contour function. The off-gaze iris image is transformed into a frontal image using an affine transform specified by θ, γ . Still, a problem of this approach is the need for an initial center, as well as the existence of boundary outliers and eyelashes.

2.4.2 Geodesic Active Contours approach

This approach, proposed by [45], is based on the relation between active contours and the computation of geodesics (minimal length curves). The strategy is to evolve an arbitrarily initialized curve from within the iris under the influence of geometric properties of the iris boundary. GACs combine the energy minimization approach of the classical “snakes” and the geometric active contours based on curve evolution.

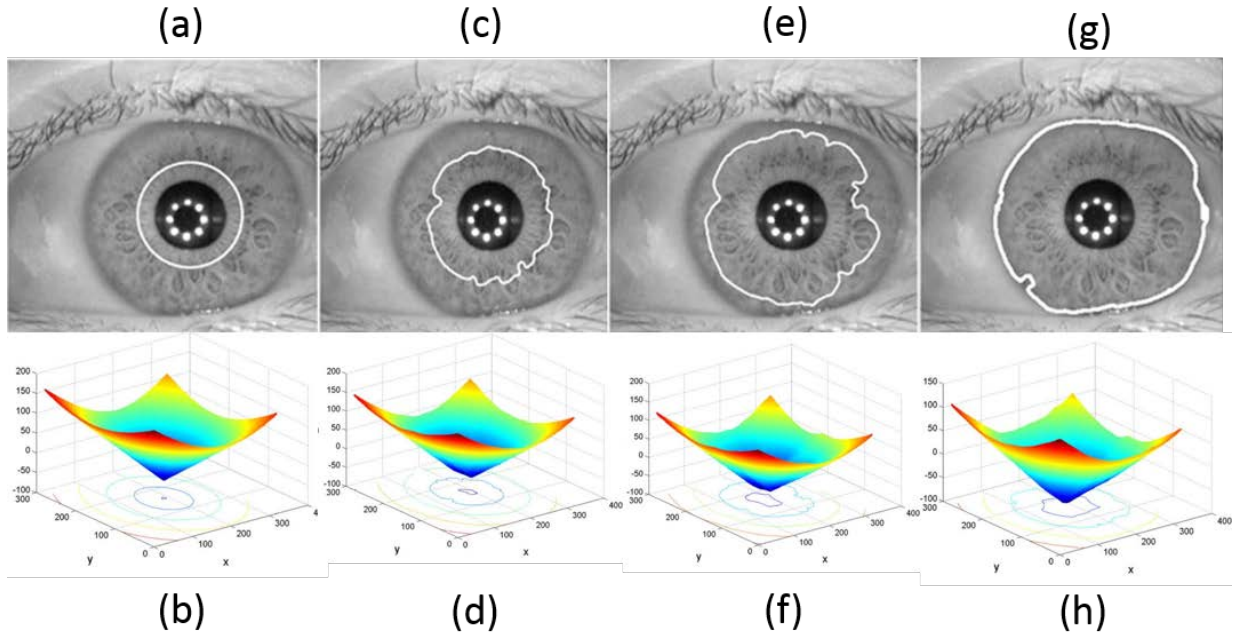


Fig. 8. Evolution of the GAC during iris segmentation. (a) Iris image with initial contour, (b) embedding function ψ (X and Y axes correspond to the spatial extent of the eye image and the Z axis represents different level sets), (c)–(f) contours after 600 and 1,400 iterations and their corresponding embedding functions, and (g), (h) final contour after 1,800 iterations. [45]

Let $\gamma(t)$ be the curve, which has to gravitate toward the outer boundary of the iris, at a particular time t . The time t corresponds to the iteration number. Let ψ be a function measuring the signed distance from the curve $\gamma(t)$. That is, $\psi(x, y) = \text{distance of point } (x, y) \text{ to the curve } \gamma(t)$.

$$\psi(x, y) = \begin{cases} 0, & \text{if } (x, y) \text{ is on the curve;} \\ < 0, & \text{if } (x, y) \text{ is inside the curve;} \\ > 0 & \text{if } (x, y) \text{ is outside the curve.} \end{cases} \quad (23)$$

Here, ψ is of the same dimension as that of the eye image $I(x, y)$. The curve $\gamma(t)$ is called the level set of the function ψ . Level sets are the set of all points in ψ where ψ is some constant. Thus, $\psi = 0$ is the zeroth-level set, $\psi = 1$ is the first level set, and so on. ψ is the implicit representation of the curve $\gamma(t)$ and is called the embedding function since it embeds the evolution of $\gamma(t)$. The embedding function evolves under the influence of image gradients and the region's characteristics so that the curve $\gamma(t)$ approaches the desired boundary of the iris. The initial curve $\gamma(t)$ is assumed to be a circle of radius r just beyond the pupillary boundary. Let the curve $\gamma(t)$ be the zeroth-level set of the embedding function. This implies that

$$\frac{d\psi}{dt} = 0,$$

by the chain rule,

$$\frac{d\psi}{dt} = \frac{\partial\psi}{\partial x} \frac{dx}{dt} + \frac{\partial\psi}{\partial y} \frac{dy}{dt} + \frac{\partial\psi}{\partial t},$$

i.e.

$$\frac{d\psi}{dt} = -\nabla\psi * \gamma'(t),$$

splitting the $\gamma'(t)$ in the normal ($N(t)$) and tangential ($T(t)$) directions,

$$\frac{d\psi}{dt} = -\nabla\psi * (v_N N(t) + v_T T(t)),$$

now, since $\nabla\psi$ is perpendicular to the tangent to $\gamma(t)$,

$$\frac{d\psi}{dt} = -\nabla\psi * (v_N N(t)). \quad (24)$$

The normal component is given by

$$N = \frac{\nabla\psi}{\|\nabla\psi\|},$$

substituting this in Eq.19

$$\frac{d\psi}{dt} = -v_N \|\nabla\psi\|.$$

Let v_N be a function of the curvature of the curve k , stopping function K (to stop the evolution of the curve) and the inflation force c (to evolve the curve in the outward direction) such that

$$\frac{d\psi}{dt} = -(\text{div} \left(K \frac{\nabla\psi}{\|\nabla\psi\|} \right) + ck) \|\nabla\psi\|.$$

Thus, the evolution equation for ψt such that $\gamma(t)$ remains the zeroth-level set is given by

$$\psi_t = -K(c + \varepsilon k) \|\nabla\psi\| + \nabla\psi \cdot \nabla K, \quad (25)$$

where K , the stopping term for the evolution, is an image-dependant force and is used to decelerate the evolution near the boundary; c is the velocity of the evolution; ε indicates the degree of smoothness of the level sets; and k is the curvature of the level sets computed as

$$k = \frac{\psi_{xx}\psi_y^2 - 2\psi_x\psi_y\psi_{xy} + \psi_{yy}\psi_x^2}{(\psi_x^2 + \psi_y^2)^{\frac{3}{2}}}.$$

Here, ψ_x is the gradient of the image in the x -direction, ψ_y is the gradient in the y -direction. ψ_{xx} is the second order gradient in the x -direction, ψ_{yy} is the second order gradient in the y -direction, and ψ_{xy} is the second-order gradient, first in the x direction and then in the y -direction. Eq (25) is the level set representation of the geodesic active contour model. This means that the level set C of ψ is evolving according to

$$C_t = K(c + \varepsilon k)N - (\nabla K \cdot N)N, \quad (26)$$

where N is the normal to the curve. The term kN provides the smoothing constraints on the level sets by reducing their total curvature. The term cN acts like a balloon force, and it pushes the curve outward toward the object boundary. The goal of the stopping function is to slow down the evolution when it reaches the boundary. However, the evolution of the curve will terminate only when $K = 0$, i.e., near an ideal edge. In most images, the gradient values will be different along the edge, thus requiring the use of different K values. In order to circumvent this issue, the third geodesic term ($(\nabla K \cdot N)$) is necessary so that the curve is attracted toward the boundary (∇K points toward the middle of the boundary). This term makes it possible to terminate the evolution process even if (a) the stopping function has different values along the edges and (b) gaps are present in the stopping function.

The stopping term used for the evolution of level sets is given by

$$K(x, y) = \frac{1}{1 + \left(\frac{\|\nabla(G(x, y) * I(x, y))\|}{k} \right)^\alpha}, \quad (27)$$

where $I(x, y)$ is the image to be segmented, $G(x, y)$ is a Gaussian filter, and k and α are constants. As can be seen, $K(x, y)$ is not a function of t .

A contour is first initialized near the pupil (Fig. 8a). The embedding function ψ is initialized as a signed distance function to $\gamma(t = 0)$ which looks like a cone (Fig. 8b). Discretizing Eq. (25) leads to the following equation:

$$\frac{\psi_{i,j}^{t+1}}{\Delta t} = -cK'_{i,j}\|\nabla\psi^t\| - K'_{i,j}(\varepsilon k_{i,j}^t\|\nabla\psi^t\|) + \nabla\psi_{i,j}^t \cdot \nabla K'_{i,j}, \quad (28)$$

where Δt is the time step. The first term ($cK'_{i,j}\|\nabla\psi^t\|$) on the right-hand side of the above equation is the velocity term (advection term) and, in the case of iris segmentation, acts as an inflation force. This term can lead to singularities and hence is discretized using upwind finite differences. The upwind scheme for approximating $\|\nabla\psi\|$ is given by

$$\begin{aligned} \|\nabla\psi\| &= \sqrt{A}, \\ A &= \min(D_x^- \psi_{i,j}, 0)^2 + \max(D_x^+ \psi_{i,j}, 0)^2, \\ A &= \min(D_y^- \psi_{i,j}, 0)^2 + \min(D_y^+ \psi_{i,j}, 0)^2, \end{aligned}$$

where $D_x^- \psi$ is the first-order backward difference of ψ in the x -direction, $D_x^+ \psi$ is the first-order forward difference of ψ in the x -direction, $D_y^- \psi$ is the first order backward difference of ψ in the y -direction, and $D_y^+ \psi$ is the first-order forward difference of ψ in the y -direction. The second term ($K'_{i,j}(\varepsilon k_{i,j}^t\|\nabla\psi^t\|)$) is a curvature-based smoothing term and can be discretized using central differences. The third geodesic term $\nabla\psi_{i,j}^t \cdot \nabla K'_{i,j}$ is also discretized using the central differences.

After evolving the embedding function ψ according to Eq. (28), the curve begins to grow until it satisfies the stopping criterion defined by the stopping function K' . But at times, the contour continues to evolve in a local region of the image where the stopping criterion is not strong. This leads to over-evolution of the contour. This can be avoided by minimizing the thin plate spline energy of the contour. By computing the difference in energy between two successive contours, the evolution scheme can be regulated. If the difference between the contours is less than a threshold (indicating that the contour evolution has stopped at most places), then the contour evolution process is terminated. The evolution of the curve and the corresponding embedding functions are illustrated in Fig. 8. Since the radial fibers may be thick in certain portions of the iris or the crypts present in the ciliary region may be unusually dark, this can lead to prominent edges in the stopping function. If the segmentation technique is based on parametric curves, then the evolution of the curve might terminate at these local minima. However, geodesic active contours are able to split at such local minima and merge again.

Active contours, unlike conventional models iris segmentation, they can assume any shape and multiple target objects simultaneously. A disadvantage may have the active contours is concerning to the stopping criterion. This is because if the iris contour edges are weak, the contour evolution could not stop and continue to grow beyond the borders of the iris, causing over-segmentation. Another aspect, to consider is computational time because, in comparison with other approaches, this is higher.

2.5 Combining strategies for iris inner and outer border localization

This section describes the methods in combination, the use of different techniques for better localization of iris boundary and decrease the time computational of the methods.

In [25] is proposed an algorithm for segmentation of iris images in less than ideal conditions. The method is divided into four stages. In the first step, the method estimates the position of the centers of the outer and inner boundary of the iris, and the two related radii. This step uses a similar technique to the Daugman's integro-differential operator described in [12]. In the second stage two image strips

containing the boundary of the inner and outer borders of the iris pattern are extracted from the input image. These strips are used to achieve a fine localization of the pixels that lie on the iris boundaries. Each strip is extracted by the radial gradient image processed around the candidate centers previously obtained. The last step of this stage is, after linearizing, the two strips of images are converted from Cartesian coordinates to Polar coordinate image. The last step is the removal of iris borders and regularization. This is accomplished with local maxima along the columns of the strip because the radial gradient tends to have high values, due to strong radial transitions in the gray level images. Regularization is achieved by a low pass filter, in order to smooth the transitions fast, to this step was used an algorithm similar to [46].

An approach based on the technique K-Means clustering is proposed in [26]. This method is divided into four main steps, a) the location of the eye in the image, b) location of the outer border of the iris, c) pupil detection and d) detection of eyelids. Eye detection is performed by using the Adaboost algorithm [47], with the goal of eliminating the area belonging to the face to ensure the segmentation accuracy. After removing the technical areas, authors used K-Means clustering based on co-occurrence histograms of gray levels. The result is an image where each gray level corresponds to a cluster. Then they applied a canny edge detector for further delineation of the outer limits. A modified Hough transform is applied to the aforementioned edge map for the external border. For detection of the pupil is used the method based on the integro-differential operator introduced by [12]. In the last step for the detection of eyelids, is presented a parabolic integro-differential operator combined with RANSAC¹, in order to restrict potential candidate parabolas.

The method proposed in [9] is another approach of hybrid techniques. This method is divided into four stages: elimination of specular reflections, estimation of the iris area, location of the inner and outer boundaries of the iris and location of the eyelids. The first stage reduces the segmentation errors caused by specular reflections. In this direction, the specular reflections are eliminated by applying a bilinear interpolation method, which employs an adaptive threshold to calculate the binary “reflections” map. The estimation of the area of the iris is performed by adopting a trained Adaboost-cascade classifier [48]. This algorithm identifies the presence of the iris in the image and performs a rough estimation of the image area occupied by the iris. The algorithm contains five layers validation and 346 Haar features extracted from local areas of different sizes. The location of the inner and outer boundaries of the iris is estimated using the algorithm proposed in [49] Pulling & Pushing, see (Fig.9). This algorithm is based on Hooke’s law. The method uses a combination of N massless springs joined at a common point O' , to estimate the center $O(x_p, y_p)$ and radius R_p parameters. Each ‘spring’ will produce a restoring force to resist its deformation. As a result, the current center is pulled or pushed until it reaches the equilibrium position. The last stage consists in the eyelid localization. The method searches the best fitting of the eyelids by using statistically established eyelid curvature models.

¹ RANSAC: Random Sample Consensus

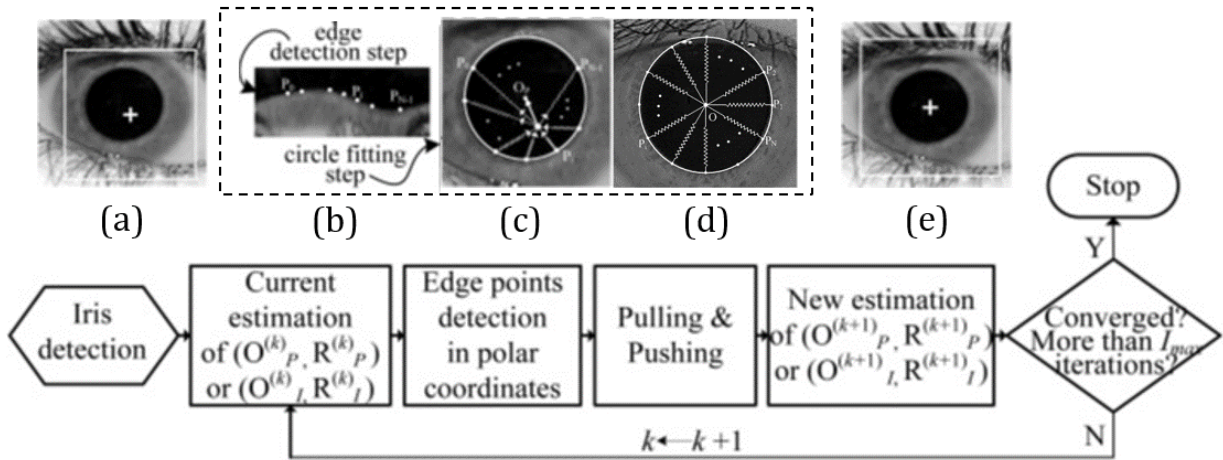


Fig. 9. The flowchart of the Pulling & Pushing (PP) method using an illustration. (a) The result of iris detection. (b) Edge detection in polar coordinates. (c) The PP forces in Cartesian coordinates. (d) The equilibrium position is reached. (e) The new estimation driven by the forces in (d) [49].

In [50] is presented another method which uses two ellipses rotated to the localization of the inner and outer boundaries of iris. This method is divided into three stages: preprocessing, location of the pupil and the estimation of the inner and outer boundaries of iris. In the preprocessing step he uses a threshold function for the location of the specular reflections, the affected areas and the intensity values are removed and interpolated. For the location of the pupil uses an algorithm based on the Hough transform, the best pupil candidate is selected based on the information of intensity and location relative to the center of the image. To estimate the inner border of the iris is employed an ellipse fitting technique, defined as:

$$\frac{\left((x - x_{p0}) \cos \varnothing + (y - y_{p0}) \sin \varnothing \right)^2}{a^2} + \frac{\left(-(x - x_{p0}) \sin \varnothing + (y - y_{p0}) \cos \varnothing \right)^2}{b^2} = 1, \quad (29)$$

where (x_{p0}, y_{p0}) is the center of the pupil and \varnothing is the angle of rotation.

In the external border used a similar method to [46] but designed for elliptic spaces. The rotated ellipses space is defined as:

$$(r, \varnothing, x_{i0}, x_{i0}): \left((x - x_{i0}) \cos \varnothing + (y - y_{i0}) \sin \varnothing \right)^2 / (ar)^2 + \left(-(x - x_{i0}) \sin \varnothing + (y - y_{i0}) \cos \varnothing \right)^2 / br^2 = 1, \quad (30)$$

where the center of the iris (x_{i0}, x_{i0}) is limited to the neighborhood of the pupil's center (x_{p0}, x_{p0}) , a and b are the parameters of the ellipse fitted into the pupil, r is the scale factor and the parameter \varnothing is set to be the angle of rotation of the pupil.

Support Vector Machines (SVM) are used by the method described in [51]. This method approximates the inner and outer iris boundaries by two circles. First, the inner boundary is estimated by an algorithm based on the Hough transform. Then, the outer boundary is estimated by using a pixel classifier based on SVM, and refined by applying the Hough transform. The used features are related to the local shape and local gradient.

In [52] is presented another method that combines several techniques for iris segmentation. It describes two different methods, an agent-based method capable of localizing the pupil's center and a method to process the iris boundaries by a multiple views approach. In the first method, an agent corresponds to the coordinates of a specific point of analysis in the input image. A population of agents is deployed in the input image, then, each agent collects local information concerning the intensity patterns visible in its region of interest. By iterations, an agent changes its position accordingly to the local properties, moving towards the estimation of the pupil center. If no available information is present in its region of interest, the agent will move itself along a random walk. After few iterations, the population tends to spread and then concentrate in the inner portion of the pupil. Once the center of the pupil has been located, the inner and outer iris boundaries are refined by an approach based on multiple views analysis. This method starts with a set of points that can be considered as an approximation of the pupil center. For each point, a detailed estimation of the iris boundaries is computed, and the final description of the iris boundaries is obtained by merging all the obtained descriptions.

Other research in this section is described in [24]. The authors proposed a novel iris segmentation method, aiming at noisy iris images in non-cooperative or less-cooperative environments. This method is divided into four different stages, removal of the specular reflections, iris area location, inner and outer boundaries detection and location of eyelid, eyelashes and shadow. To solve the problem related to disposing of specular reflections, is performed by using the algorithm described in [9]. The second step aims to obtain a rough estimation of the iris area and to identify the non-iris regions (e.g. eyelashes and eyebrows). This step is performed by using a clustering technique based on two different algorithms. The first one creates the clusters by using the intensity information and then expands the area of these clusters by using an iterative technique. The second algorithm performs a semantic refinement in order to identify the candidate iris region and the non-iris regions. This algorithm tries to label the different areas of the image by using the information related to the shape, intensity and position of each clustered region. The estimation of the inner and outer iris boundaries is performed by using an algorithm based on the integro-differential operator presented in [12]. This algorithm aims to speed up the segmentation based on the integro-differential operator and to limit the problems related to the presence of local optima in the image. The algorithm iteratively searches the shortest path by using a technique that considers the results obtained applying the integro-differential operator in a constellation of near points. In the latter step of this technique inaccuracies in the location are detected and eliminated through current statistics. The last stage is the location of the eyelids, where it is used an algorithm similar to that proposed in [9], based on a horizontal 1-D rank filter and an eyelid curvature model.

A combined method is proposed in [27] for the pupil estimation. The method combines active contours and Pulling & Pushing modified method [49]. The method is composed of four main areas: (a) division of the convergence in two phases: coarse and fine; (b) utilization of min & max – Active Contour as edge detector; (c) calculation of the length of the springs; (d) modification of the convergence criteria. The method starts its execution in the coarse phase, with the initial estimation at image center, in this phase; the algorithm computes the minimum distance between the center and the image edges. In the fine contour phase, the radial direction is limited to $(r_{max} = \overline{R}^l + \Delta r)$, where \overline{R}^l is the mean radius from the previous iteration and Δr is a constant, forcing the transformed image to have both pupil and iris regions. In the second stage, is applied the min & max – Active Contour to detect the edges and consequently, to find the size of the springs in relation to the center. In the fourth stage defines a way to calculate the size of the springs. As the end result is an active contour area, its boundaries are extracted. The length of the spring is calculated for each direction, as the average value of the boundary points in this direction. In directions in which the boundaries are not defined an interpolation scheme is applied. And finally, the method ends when it meets the modified stopping criterion.

2.6 Other Iris segmentation methods

[53];[54] use a bisection method to locate the center of the pupil. The center of the pupil is used as reference to detect the inner and outer boundaries of the iris. First, edge detection is applied to the iris image to extract the edge information. For every two points on the same edge component, a bisection method is applied to draw the perpendicular lines to the center point. The center point with a maximum number of line intersections is selected as the center of the pupil. A virtual circle is drawn with reference to the center of the pupil and the radius is increased within a certain range. Two virtual circles with the largest number of edge points are chosen as the inner and outer boundaries of the iris.

In [55] is proposed a method which applies mathematical morphology to a polar/radial-invariant image filtering and to a circular segmentation using shortest paths from generalized grey-level distances. This algorithm is composed of five steps, color component selection, reflection removal, outer boundary localization, and inner boundary localization. In the first step, it first performs the selection of the most appropriate grayscale values of the image to the segmentation of the different elements. This selection is based primarily on the choice of the RGB components having the maximum entropy of the histogram. To eliminate reflections, it uses an opening operator and thresholding task. In the estimation of the external border of the iris, combines two close-hole operators and image inversions to estimate the center. For that, it gets the maximum distance from the distance calculation widespread gray level of the border on the residue of the original image and filled image. Then the image is converted to polar coordinates, the visibility of the border is enhanced by applying a morphological multiscale gradient and an anisotropic averaging filter. Finally, there is the suppression of the eyelids and eyelashes through a very simple model that refines the segmentation; the main objective being to cut the top with a straight line. The last step in the localization of the inner boundary is performed by a procedure similar to the detection of the external border of the iris. The center of the pupil is refined using the close-holes operator and grey-level generalized distance from the prior iris segmentation. The pupil is then segmented using the circular minimal-path obtained from the polar transformation of the reflection-free image.

Black hole search method is used to compute the center and area of a pupil [56];[57]. Since the pupil is the darkest region in the image, this approach applies threshold segmentation method to find the region. Firstly, a threshold is defined to identify the dark areas in the iris image. The dark areas are called as “black holes”. The center of mass of these black holes is computed from the global image. The area of pupil is the total number of those black holes within the region. The radius of the pupil can be calculated from the circle area formula. Black hole search method is not suitable for iris image with dark iris. The dark iris area would be detected instead of the area of pupil.

The method proposed in [58] performs the iris recognition using iris images captured by a special device composed by two CCD sensors, which simultaneously capture an infrared image and an RGB color image. This system uses the color image in order to better perform the segmentation step. The inner and outer iris boundaries are estimated by using two different algorithms. The inner iris boundary is estimated by considering only the infrared image. First, a rough representation of the pupil area is obtained by using a method based on the search of dark pixels. Then, the outer iris boundary is estimated by using a direct least square fitting of the ellipse [59]. The outer iris boundary estimation considers the information related to both, the infrared image and the RGB image. For each color channel, the edges are extracted by using the Canny algorithm. A trained classifier is then adopted in order to remove the noisy edge points. The outer iris boundary is finally estimated as a circumference by applying the RANSAC technique. An algorithm similar to the one proposed for the estimation of the outer iris boundary is then used for estimating the shape of the eyelids. This algorithm is based on the RANSAC technique for the searching of parabolic shapes.

The iris segmentation is usually performed in two steps: first the inner and outer boundaries of the iris region are estimated, then occlusions and reflections are detected and removed. It is possible to divide the methods for the estimation of the inner and outer iris boundaries in five classes: methods based on Daugman’s integro-differential operator, methods based in the Hough Transform, iterative

methods, active contours methods, combining strategies for iris segmentation and methods that do not fall in any of the above mentioned classes.

The methods based on Daugman's Integro-differential operator and the Hough Transform; perform the approximation of the boundaries by two circumferences. The iterative methods for iris segmentation are based on running a few rounds to converge to the solution. These methods begin by selecting a random starting point to find the region of interest, from this point begins to iterate and to better estimate more refined iris boundaries. Also the methods based on active contours do not perform assumptions regarding the iris shape. These methods combine an iterative contour growing with shape constraints, in order to better match the boundaries of the iris without introducing noise errors due to local image variations. Differently, the combining strategies, as the name suggests, combine techniques from different classes, performing the iris segmentation in an incremental way. Other methods are not easily classifiable, such as a method designed for a special biometric device, a method that performs the iris segmentation by using morphological operators, and a method that combines different new algorithms.

3 Segmentation of noisy Iris images methods

This sections reviews the methods especially designed to remove reflections, shadows, and occlusions (such as eyelids and eyelashes) from the iris image. The methods designed to remove the specular reflections are based, primarily, on frequency analysis methods and methods based on thresholds the image intensity. The majority of the methods for the segmentation of eyelids and eyelashes are based on edge detectors, local variance thresholding, or intensity thresholding.

Texture segmentation is adopted to detect upper and lower eyelids in [16]. The high spectrum energy is used to compute the eyelashes segments. The region with high frequency is considered as the eyelash area. The information of the pupil position is used in upper eyelash segmentation. The upper eyelashes are fit with a parabolic arc. The parabolic arc shows the position of the upper eyelid. For lower eyelid detection, the histogram of the original image is used. The lower eyelid area is segmented to compute the edge points of the lower eyelid. The lower eyelid is fit with the edge points.

In [60], the Daubechies wavelets method is used to decompose the original image into four bands, HH, HL, LH and LL. Canny edge detection is applied to the LH image. To minimize the influence of eyelashes, Canny edge detector is tuned to horizontal direction. The edge points that are close to each other are connected to detect the upper eyelid. The longest connected edge that fits with a parabolic arc is taken as the upper eyelids. To detect lower eyelid, the steps are repeated with lower iris boundary area.

A method to eliminate reflections and eyelashes is presented in [25] to improve the segmentation process. For this, the method is divided into three main steps, the first method estimates the presence of the eyelashes, after identifying the presence of reflections and finally marked occlusions are estimated and removed. In the first step two different eyelashes are considered to distinguish separable and non-separable. For detection of eyelashes separable Gabor filter is applied to extract the most distinguishing features of the eyelashes. While a thresholding method based on the highest values of local variation is employed for the detection of non-separable eyelashes. For the identification of reflections they are distinguished in weak and strong reflections. The weak reflections are detected by thresholding the regions with high local variance values, while strong reflections are detected by considering the intensity levels greater than a fixed threshold. Finally applies an iterative technique of growing region, in order to correctly fuse each data segmentation mask.

The method proposed by [30] uses a threshold operation applied to the image, where the threshold T_{ref} is set at a fixed ratio P between the average value I_{ave} and the maximum value I_{max} of the image intensity. The threshold value is individually calculated for each image based on the histogram, as shown in Eq. (31). Then the map of reflections obtained is improved by morphological operations.

$$T_{ref} = I_{ave} + P * (I_{max} - I_{ave}) \quad \text{where } P \in (0, 1). \quad (31)$$

Gabor filter and variance of intensity approaches are proposed for eyelash detection [61]. The eyelashes are categorized into separable eyelashes and multiple eyelashes. Separable eyelashes are detected using 1D Gabor filters. A low output value is obtained from the convolution of the separable eyelashes with the Gabor filter. For multiple eyelashes, the variance of intensity is very small. If the variance of intensity in a window is smaller than a threshold, the center of the window is considered as the eyelashes.

The methods described in [24];[9] first performs the estimation of the borders (top and bottom) of the eyelids, then eyelashes and shadows are detected. The positions of the eyelids are first estimated by considering the results of a rough searching of the eyelashes. Like most of eyelashes are similar in shape (vertical, thin and dark), adopted an algorithm for the location of the eyelids with a 1-D horizontal rank filter removes the eyelashes. The horizontal rank filter provides a clearer vertical limit, so it helps to detect edge of the eyelid. This allows detection of edge points along the vertical direction. Then, an edge map is obtained which is refined through a statistical model of curvature, which are two parabolic arcs. For detection of eyelashes and shadows they used a model that provides an adaptive threshold for eyelash and shadow detection by analyzing the local intensity distributions of different iris regions.

According to [62], both the edge and region information are used for noise detection. To speed up iris segmentation, the iris is roughly localized using filtering, edge detection and Hough transform. The localized iris is normalized to rectangular block. A bank of Gabor filters is used to extract the edge information based on phase congruency. The obtained edge information is combined with the region information to detect the eyelashes and pupil noise regions.

[63] describe the methods used to detect the eyelids and eyelashes. First for the estimation of the eyelids, after locating the inner and outer boundaries of the iris they use the two cross points between the upper eyelid and the upper boundary. Then the eyelids candidate points are extracted by using an eyelid detection mask. After extracting eyelid candidate point parabolic Hough transform is used to more accurately locate the detection limits of the eyelids. As an initial position for detection of the eyelashes it takes the detected eyelid line. Eyelashes are classified in two types: separate eyelashes and multiple eyelashes or no-separated eyelashes. The proposed algorithm for the detection of separate eyelashes adopts a convolution kernel. The multiple eyelashes are detected by a local window, threshold intensity and standard deviation values.

In order to detect the eyelids and eyelashes [64] presents, eight models eyelids /eyelashes and eight sub-blocks with fixed size. The maximum deviation of each sub-block is calculated (top and bottom of the iris) seeking the model that best fits, using equations (32) and (33):

$$\sigma_{up}(n) = \max \left\{ \sum_{i=nx9+1}^{nx9+9} \sum_{j=45+\theta}^{135+\theta} (I(i, j + \theta) - \bar{R})^2 \right\}, \quad (32)$$

$$(|I(i, j + \theta) - \bar{R}| \geq \sigma_R + 20, \theta = -9, -8, \dots, 9)(n = 0, 1, \dots, 7).$$

$$\sigma_{bottom}(n) = \max \left\{ \sum_{i=nx9+1}^{nx9+9} \sum_{j=225+\theta}^{315+\theta} (I(i, j + \theta) - \bar{R})^2 \right\}, \quad (33)$$

$$(|I(i, j + \theta) - \bar{R}| \geq \sigma_R + 20, \theta = -9, -8, \dots, 9) (n = 0, 1, \dots, 7).$$

Where \bar{R} and σ_R are the intensity mean and deviation of reference iris areas. The θ is the translation which can compensate the iris image rotation in polar coordinates. The n is the sequence number of each sub-block and for each sub-block there is a maximum σ_n with different θ .

In [65] they propose a precise method for the detection of eyelids, eyelashes and refining mask based on morphology. The method segments the image by using the connectivity of the lashes which is the base for the region's growth, this being an important preliminary information. Based on this characteristic, it was proposed that regional growth principles could maximize the region that is occluded by eyelashes and eyelids. (Fig. 10) shows the types of noises in the image of iris. Region growing is a procedure that growing pixel or sub-regions into larger regions based on predefined criteria, The basic approach is to start with a set of "seed" points and from these grow regions by appending to each seed those neighboring pixels that have properties similar to the seed (such as specific ranges of gray level).

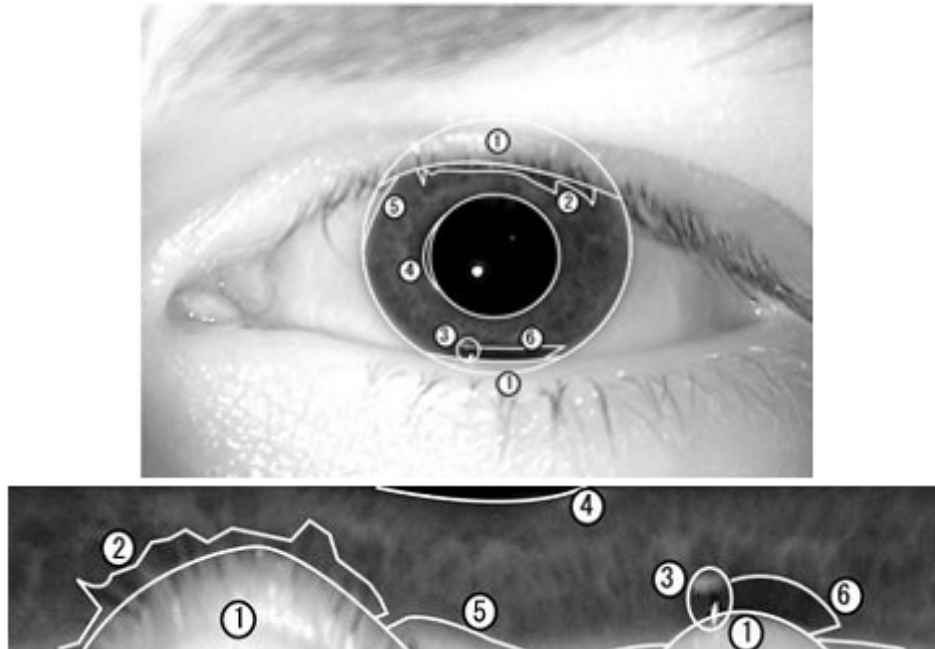


Fig. 10. Top: Occluded iris regions found in Cartesian domain. The numbers in this figure correspond to, 1) eyelids, 2) eyelashes, 3) specular reflections, 4) pupil, 5) sclera, and 6) shadow caused by an eyelid. Bottom: Iris occlusion regions found in polar domain. The numbers in the bottom figure correspond to the noise types in the top Figure.[65]

Thus the pixel with the lowest intensity value is then chosen as the starting point for a region growing process. New pixels belonging to the region are linked to the growing region if the absolute difference between their intensities is below than a fixed threshold.

In Alonso-Fernandez and Bigun[66] propose an approach, which takes into account the quality factors affecting image iris segmentation. Due to this, the impact of 8 quality measures in the performance of segmentation is evaluated. These are calculated locally (around the pupil) and globally (in the whole image), these measures below mentioned and calculating of some are described briefly, For more details see [66]. The quality measurements used are sharpness (defocus blur), motion blur and interlace, contrast of the iris boundaries, circularity of iris boundaries, propagation grayscale, and occlusion. Sharpness is measured with the method proposed in [67], which calculates the amount of high frequency components. Motion blur is measured with two parameters: direction (angle) and number of pixels- smear (force). The adjacent rows are used for motion blur measurement because they are quite different in images with motion blur. The contrast of the iris boundaries is quantified by two means: the Edge Sharpness of Iris[68] (IES) and Orientation Certainty Level[69] (OCL). IES is

computed from two points equidistant on either side of the circle and the second measure is used to quantify the strength of the iris pupil and iris contour transitions to the sclera.

For the segmentation an algorithm based on the Generalized Structure Tensor is used. This algorithm takes into account the direction of the edges as well as the correlation of edges magnitude. By using complex filters encoding local orientation of the sought (circular) pattern, its response is penalized if there is disagreement of local image orientations with the filter.

4 Discussion and challenging about iris segmentation

This section provides an analysis of the most important results of the algorithms reported in the literature, in order to identify potential lines for further work. Well as a summary of the databases most used in these experiments, how they are distributed and some of its most important features.

4.1 Iris images databases

Iris-image databases are crucial to the development and advancement of iris-based biometrics. These databases along with prescribed evaluation methodologies allows for direct comparison of iris segmentation or recognition algorithm performance. The databases will increase in size and complexity of iris-image until all algorithmic problems, inefficiencies, and shortcomings have been fully addressed [70].

Advances in the state-of-the-art on iris recognition have led to the emergence of a lot of databases, either as part of challenges or published for public use. The closed or proprietary databases, are difficult to acquire for the study of biometric systems with the aim of demonstrating their performance, public or free datasets are a valuable means to compare existing approaches.

The perfect iris-image database should be sufficiently large, consist of images collected from a large and heterogeneous group of subjects, and contain images that depict noise factors typically encountered in real world applications [70]

According to [71], the biometric databases should have the following properties:

- ❖ Relevant (large number of samples within the class, i.e. the same person, in the identification mode).
- ❖ Large (size should exceed the lower limit needed to support the required accuracy).
- ❖ Representative (vary in gender, age and other demographic characteristics).
- ❖ Targeted (with respect to the specific types of sensors, models, etc.).
- ❖ Tagged (provide meta-information).
- ❖ Time-variant (characteristics are captured during large time periods).
- ❖ Un-edited (without post-processing).

With these properties, several biometric databases are available for iris recognition. The Table 3 shows a list of the most used iris database with detailed specifications. These iris databases are available and free for research purposes.

Table 3. Overview of common open iris databases free for research purposes. Take it from [72].

Dataset	Type	Size	Format	Images	Classes	Sensor
CASIA						
Db-Casia.v1	NIR	320x280	BMP	756	108	Casia-CAM
Db-Casia.v2	NIR	640x480	BMP	2x1,200	2x60	OKI Irispass-H; Casia-CAM v2
Db-Casia.v3 Interval	NIR	320x280	JPG	2,639	395	Casia-CAM
Db-Casia.v3 Lamp	NIR	640x480	JPG	16,212	819	OKI Irispass-H
Db-Casia.v3 Twins	NIR	640x480	JPG	1,183	400	OKI Irispass-H

Db-Casia.v4 Interval	NIR	320x280	JPG	2,639	395	Casia-CAM
Db-Casia.v4 Lamp	NIR	640x480	JPG	16,212	819	OKI Irispass-H
Db-Casia.v4 Twins	NIR	640x480	JPG	1,183	400	OKI Irispass-H
Db-Casia.v4 Distance	NIR	2,352x1,728	JPG	2,639	395	Casia-LR-CAM
Db-Casia.v4 Thousand	NIR	640x480	JPG	20,000	2,000	IrisKing IKEMB-100
Db-Casia.v4 Syn	NIR	640x480	JPG	10,000	1,000	(N/A)Synthetic
ICE						
Db-ICE.2005	NIR	640x480	TIFF	2,953	132	LG 2200
Db-ICE.2006	NIR	640x480	TIFF	59,558	480	LG 2200
MMU						
Db-MMU.1	NIR	320x240	BMP	450	92	LG 2200
Db-MMU.2	NIR	320x238	BMP	995	200	Panas BM-ET100
ND						
Db-ND-Cross Sensor	NIR	640x480	TIFF	264,945	1,352	LG 2200 + LG 4000
Db-ND-Iris- 0405	NIR	640x480	TIFF	64,980	712	LG 2200
UBIRIS						
Db-Ubiris.v1	VW	200x150	JPEG	1,877	246	Nikon E5700
Db-Ubiris.v2	VW	400x300	TIFF	11,102	522	Canon 5D
WVU						
Db-WVU-Biomdata.v1	NIR	640x480	BMP	3,043	462	OKI Irispass-H
Db-WVU-Biomdata.v2	NIR	640x480	BMP	763	144	OKI Irispass-H
Db-WVU-OffAxis	NIR	720x480	JPG;TIFF	268	38	Sony DSC-F717
OTHERS						
Db-Bath	NIR	1280x960	J2K	1,600	800	ISG-LW-1.3S-1394
Db-IITD.v1	NIR	320x240	BMP	1,120	224	JIRIS JPC100
Db-MBGC-NIR Video	NIR	2,000x2,000	Video	571	-	MBGC-Portal
Db-UPOL	VW	576x768	PNG	384	128	TOPCON TRC50IA + Sony DXC-950P

4.1.1 CASIA-Iris

- Db-CASIA.v1:** [<http://biometrics.idealtest.org/dbDetailForUser.do?id=1>]. It is an iris database provided by National Laboratory of Pattern Recognition, Institute of Automation, Chinese Academy of Sciences freely for iris recognition researchers. Iris images of CASIA-IrisV1) were captured with a homemade iris camera. Eight 850nm NIR illuminators are circularly arranged around the sensor to make sure that iris is uniformly and adequately illuminated. In order to protect our IPR in the design of iris camera (especially the NIR illumination scheme) before appropriate patents were granted, the pupil regions of all iris images in CASIA-IrisV1 were automatically detected and replaced with a circular region of constant intensity to mask out the specular reflections from the NIR illuminators before public release. Clearly, such processing may affect pupil detection but has no effects on other components of an iris recognition system such as iris feature extraction since iris feature extraction only uses the image data in the region between the pupil and the sclera, i.e. the ring-shaped iris region.
The database includes 756 iris images from 108 eyes. For each eye, 7 images are captured in two sessions with our self-developed device CASIA close-up iris camera (Fig.1), where three samples are collected in the first session (Fig.2(a)) and four in the second session (Fig.2(b)). All images are stored as BMP format with resolution 320*280.
- Db-CASIA.v2:** [<http://biometrics.idealtest.org/dbDetailForUser.do?id=2>]. It was used for the First Biometrics Verification Competition (BVC) on face, iris, and fingerprint recognition in the 5th Chinese Conference on Biometrics Recognition (Sinobiometrics 2004), held in GuangZhou, China in 2004. CASIA-IrisV2 includes two subsets captured with two different devices: Irispass-H

developed by OKI and they self-developed device CASIA-IrisCamV2. Each subset includes 1200 images from 60 classes.

- **Db-CASIA.v3:** [<http://biometrics.idealtest.org/dbDetailForUser.do?id=3>]. It was used in the experimental evaluation of the iris indexing techniques proposed by [Mukherjee and Ross, 2008]. This database includes three subsets which are labeled as CASIA-Iris-Interval, CASIA-Iris-Lamp and CASIA-Iris-Twins. CASIA-Iris.v3 contains a total of 22,034 iris images from more than 700 subjects. All iris images are 8 bit gray-level JPEG files, collected under near infrared illumination. Almost all subjects are Chinese except a few in CASIA-Iris-Interval. Because the three data sets were collected in different times, only CASIA-Iris-Interval and CASIA-Iris-Lamp have a small overlap in subjects.
 - ✓ DB-CASIA.v3-Interval: Iris images of CASIA-Iris-Interval were captured with a self-developed close-up iris camera. The most compelling feature of this iris camera is that it have designed a circular NIR LED array, with suitable luminous flux for iris imaging. Because of this novel design, this iris camera can capture very clear iris images. CASIA-Iris-Interval is well-suited to study the detailed texture features of iris images.
 - ✓ DB-CASIA.v3-Lamp: CASIA-Iris-Lamp was collected using a hand-held iris sensor produced by OKI. A lamp was turned on/off close to the subject to introduce more intra-class variations when we collected CASIA-Iris-Lamp. Elastic deformation of iris texture due to pupil expansion and contraction under different illumination conditions is one of the most common and challenging issues in iris recognition. So CASIA-Iris-Lamp is good for studying problems of non-linear iris normalization and robust iris feature representation.
 - ✓ DB-CASIA.v3-Twins: CASIA-Iris-Twins contains iris images of 100 pairs of twins, which were collected during Annual Twins Festival in Beijing using OKI's IRISPASS-h camera. Although iris is usually regarded as a kind of phenotypic biometric characteristics and even twins have their unique iris patterns, it is interesting to study the dissimilarity and similarity between iris images of twins.
- **Db-CASIA.v4:** [<http://biometrics.idealtest.org/dbDetailForUser.do?id=4>]. It is an extension of CASIA-IrisV3 and contains six subsets. The three subsets from CASIA-IrisV3 are CASIA.v3-Iris-Interval, CASIA.v3-Iris-Lamp and CASIA.v3-Iris-Twins respectively. The three new subsets are CASIA.v4-Iris-Distance, CASIA.v4-Iris-Thousand, and CASIA.v4-Iris-Syn.
 - ✓ DB-CASIA.v4-Distance: CASIA-Iris-Distance contains iris images captured using a self-developed Long-range Multi-modal Biometric image acquisition and recognition System (LMBS). The advanced biometric sensor can recognize users from 3 meters away by actively searching iris, face or palmprint patterns in the visual field via an intelligent multi-camera imaging system. The LMBS is human-oriented by fusing computer vision, human computer interaction and multi-camera coordination technologies and improves greatly the usability of current biometric systems. The iris images of CASIA-Iris-Distance were captured by a high resolution camera so both dual-eye iris and face patterns are included in the image region of interest. And detailed facial features such as skin pattern are also visible for multi-modal biometric information fusion.
 - ✓ DB-CASIA.v4-Thousand: CASIA-Iris-Thousand contains 20,000 iris images from 1,000 subjects, which were collected using IKEMB-100 camera produced by IrisKing (<http://www.irisking.com>). IKEMB-100 is a dual-eye iris camera with friendly visual feedback, realizing the effect of “What You See Is What You Get”. The bounding boxes shown in the frontal LCD help users adjust their pose for high-quality iris image acquisition. The main sources of intra-class variations in CASIA-Iris-Thousand are eyeglasses and specular reflections. Since CASIA-Iris-Thousand is the first publicly available iris dataset with one thousand subjects, it is well-suited for studying the uniqueness of iris features and develop novel iris classification and indexing methods.

- ✓ **DB-CASIA.v4-Syn:** CASIA-Iris-Syn contains 10,000 synthesized iris images of 1,000 classes. The iris textures of these images are synthesized automatically from a subset of CASIA-IrisV1 with the approach described in [Tan, et al., 2010]. Then the iris ring regions were embedded into the real iris images, which makes the artificial iris images more realistic. The intra-class variations introduced into the synthesized iris dataset include deformation, blurring, and rotation, which raise a challenge problem for iris feature representation and matching. In [Tan, et al 2010] was demonstrated that the synthesized iris images are visually realistic and most subjects can not distinguish genuine and artificial iris images. More importantly, the performance results tested on the synthesized iris image database have similar statistical characteristics to genuine iris database. So users of CASIA-IrisV4 are encouraged to use CASIA-Iris-Syn for iris recognition research.

4.1.2 ICE

- **Db-ICE.2005:** ICE mean Iris Challenge Evaluations. The National Institute of Standards and Technology (NIST), [73], has provided researchers the database ICE.2005. This database consists of 2953 grayscale eye images of 132 people. They are acquired with a dedicated LG2200 camera. Each image captures one eye and has a size of 640x480 pixels. This database has been divided into two sub-databases : one for images of the right iris (1425 iris images from 124 persons) and another one for images of the left iris (1528 iris image of 120 persons). In most cases, images of the right and left irises are acquired at the same time. This database contains images with a wide range of visual quality; some images seem near perfect while others are very blurry, have iris that extend off the periphery of the image, contain significantly occluded irises, and/or have video interlace artifacts.
- **Db-ICE.2006:** The database of iris images ICE.2006 is an extension of the ICE.2005 database . The images in the ICE.2006 intentionally represent a broader range of quality than the ICE 2006 sensor would normally acquire. This includes images that did not pass the quality control software embedded in the sensor. The database is composed by 59 558 images collected from 480 subjects. The images are all VGA resolution, 480 rows by 640 columns, with 8-bit grayscale resolution.

4.1.3 MMU

- **Db-MMU.v1:** The Multimedia University has developed MMU1 [74] iris database contributes a total number of 450 iris images which were taken using LG IrisAccess 2200. This camera is semi-automated and it operates at the range of 7-25 cm.
- **Db-MMU.v2:** The MMU2 [74] iris database consists of 995 iris images. The iris images are collected using Panasonic BM-ET100US AuthentiCam and its operating range is even farther with a distance of 47-53 cm away from the user.
These iris images are contributed by 100 volunteers with different age and nationality. They come from Asia, Middle East, Africa and Europe. Each of them contributes 5 iris images for each eye. There are 5 left eye iris images which are excluded from the database due to cataract disease. Obviously, the images are highly homogeneous and their noise factors are exclusively related with small iris obstructions by eyelids and eyelashes

4.1.4 ND

- **Db-ND-Cross Sensor:** The Notre Dame University ND-CrossSensor-Iris-2012 Dataset [75]. This dataset was initially released for the Cross Sensor Iris Recognition Challenge associated with the BTAS 2012 conference [<https://sites.google.com/a/nd.edu/btas2012crosssensoririscompetition/>]. This dataset occupies about 104 GBytes, and consists of 27 sessions of data with 676 unique subjects. An average session contains 160 unique subjects which have multiple images from both the LG2200 and LG4000 iris sensors. There are 29939 images from the LG4000 and 117503 images from the LG2200. Every subject occurs in at least two sessions across the entire data set. This data set spans

three years, 2008 to 2010. The initial images are taken from both sensors and are 640 by 480. There are additional images included in this data set, known as the modified LG2200 images. The original images have been stretched vertically by 5% to compensate for the non-unit aspect ratio of the digitizer used in the LG2200 computer-hosted runtime acquisition system (this elongation was suggested by Imad Malhas of IrisGuard Inc. in 2009). Hence these additional images are of size 640 by 504.

- **Db-ND-Iris-0405:** The Notre Dame University ND-IRIS-0405 Iris Image Dataset [76]. The data set contains 64,980 iris images obtained from 356 subjects (712 unique irises) between January 2004 and May 2005.

The age range of the subjects is 18 to 75 years old. 158 of the subjects are female, and 198 are male. 250 of the subjects are Caucasian, 82 are Asian, and 24 are other ethnicities. None of the images correspond to subjects wearing glasses during image acquisition. However, a significant fraction of the subjects wore contact lenses. Image artifacts arising from contact lenses are discussed in a later section. All images were acquired using the same LG 2200 iris biometrics system. The LG 2200 uses near-infrared illumination of the eye, and provides audible prompts to help the subject position their head appropriately for image acquisition.

4.1.5 UBIRIS

- **Db-UBIRIS** database created by the SOCIA Lab. (Soft Computing and Image Analysis Group) of the Department of Computer Science, University of Beira Interior, Portugal [77]. This database was presented in 2 versions.

- ✓ UBIRIS.v1 database (2004) [78] is comprised of 1877 images collected from 241 persons in two distinct sessions. This database incorporates images with several noise factors, simulating less constrained image acquisition environments. Since September 2005, this database has been freely downloaded by more than 500 individuals and institutions from over 70 different countries and its data constituted the basis for a large number of works with academic, research and commercial purposes.
- ✓ UBIRIS.v2 database is the second version of the UBIRIS database [79]. This database has significantly more images and with new and more realistic noise factors, when compared to its predecessor. Both databases contain visible wavelength iris images captured in heterogeneous lighting conditions, with strong appearance of highly degraded images [80].

4.1.6 WVU-Biomdata

- **Db-WVU-Biomdata.v1:** The West Virginia University multimodal biometric dataset collection (BIOMDATA), collects iris, fingerprint, palm-print, voice and face data from over 200 people [81]. The data was collected using standard enrolment devices, where possible, such as the SecuGen optical fingerprint biometric scanner, the OKI IRISPASS-h handheld device for the iris, and the IR Recognition Systems HandKey II for hand geometry with image and sound recordings for face and voice, respectively. The dataset also includes soft biometrics such as height and weight, for subjects of different age groups, ethnicity and gender with variable number of sessions/subject.

First release of the biometric dataset collection contains image and sound files for six biometric modalities: Iris, face, voice, fingerprint, hand geometry and palm print.

OKI IRISPASS-h handheld device is used to capture the image of the iris. The user is asked to hold the device away from one eye (at a distance eyeglasses would be away from the face) while covering the other eye with the hand; the covered eye must remain open, so that the pictured eye does not squint. The user should be able to see all sides of the green box displayed on the screen of the biometric device. The software used is provided by the constructor of the biometric scanner. The size of the iris picture is 302 KB, 480×640 and 2 KB for the .log file that contains the setup parameters of the biometric scanner. Four images of each eye are taken during one session. At the discretion of the

volunteer more data samples were acquired when subjectively was determined that the quality of the image was poor. First release of the iris biometric dataset contains 3043 bmp iris images.

- **Db-WVU-Biomdata.v2:** Second release of the biometric dataset collection contains image and video files for the following modalities [81]: Iris; Face; Face video and voice; Fingerprint; Hand geometry; Palmprint. The dataset also includes soft biometrics such as height and weight, for subjects of different age, ethnicity and gender with variable number of sessions/subject. The size of the iris picture is 302 KB, 480×640 and 2 KB for the .log file that contains the setup parameters of the biometric scanner. Second release of the iris biometric dataset contains 763 bmp iris images.
- **DB-WVU-OffAxis:** Offaxis/angle iris dataset [82] contains images collected with two cameras, a Sony Cyber Shot DSC F717 and a black and white, monochrome camera (Table 4). The angles are as accurate as the subject can hold their eye in position. The Sony camera was used in infrared mode, called night vision. However, while the camera was still in night vision mode, it still used all three RGB sensor data hence the green hue to the images.

Table 4. Characteristics of WVU-OffAxis database.

Deive	Sony Cyber Shot DSC F717	Monochrome Camera
Number of Sessions	1	1
Number of Subjects	19	73
Eye	Left & Right	Left & Right
Gaze direction (angle in degrees)	0,15,30	0,15,30,0
Number of files	268	597
Image Type	JPG, TIF	BMP
Spectrum	Infrared mode (night vision)	Visible mode
Distance Eye-camera	~4 inches	~4 inches
Illumination	Ceiling, ambient office lighting	Ceiling, ambient office lighting
Location	Indoor	Indoor

4.1.7 Other public databases

- **Db-Bath:** The BATH iris database [83] was designed to obtain very high quality iris images. The initial objective was to capture 20 images from each eye of 800 subjects. The commercially available database is now twice this size. A majority of the database is comprised of students from 100 different countries and staff from the University of Bath. The images are of a very high quality taken with a professional Machine Vision Camera with infrared illumination and a consistent image capture setup.
- **Db-UPOL:** The UPOL iris image database was built within the Palacký University of Olomouc [84], Czech Republic. Its images have the singularity of being captured through an optometric framework (TOPCON TRC50IA) and, due to this, are of extremely high quality and suitable for the evaluation of iris recognition in completely noise-free environments. The database contains 384 images extracted from both eyes of 64 subjects (three images per eye). Its images have maximum homogeneity and inclusively the iris segmentation is facilitated by the dark circle that surrounds the region corresponding to the iris. Obviously, these characteristics make this database the less appropriate for the non-cooperative iris recognition research.
- **Db-IITD.v1:** The IIT Delhi Iris Database [85] mainly consists of the iris images collected from the students and staff at IIT Delhi, New Delhi, India. This database has been acquired in Biometrics Research Laboratory during Jan - July 2007 using JIRIS, JPC1000, and digital CMOS camera. The image acquisition program was written to acquire and save these images in bitmap format and is also freely available on request. The currently available database is from 224 users, all the images are in bitmap (*.bmp) format. All the subjects in the database are in the age group 14-55 years comprising of 176 males and 48 females. The database of 1120 images is organized into 224

different folders each associated with the integer identification/number. The resolution of these images is 320 x 240 pixels and all these images were acquired in the indoor environment.

- **Db-MBGC-NIR Video:** The NIR face videos of the Multi Biometric Grand Challenge (MBGC) database [86]. The database was constructed by capturing the facial videos of subjects walking through a portal. The videos have a spatial resolution of 2048 x 2048 pixels recorded in the AVI format with a frame rate of 15 frames per second (fps). Even though the extracted frames are of a very high resolution, the average usable spatial extent of the iris is about 120 pixels. The database contains 149 videos collected from 114 distinct subjects.

4.2 Comparison of existing methods

The Daugman's integro-differential operator is one of the most used methods in most of the iris recognition systems either deployed commercially or in trials, comparisons being made based on the algorithm since this has a very complex operation. It is also important to highlight the vulnerabilities of the algorithm in the presence of lighting within the pupil. Another issue here is determining the edge of the pupil, the maximum change must occur at the boundary between the iris and the dark pupil, which is relatively darker than the bright spots of illumination. Therefore, during the analysis of the image, you have to be careful that the value of the very bright spot may confuse the operator and can result in a maximum slope. Also methods based on active contours do not make assumptions about the shape of the iris. These methods combine a contour iterative increasingly constrained form, in order to better adapt to the limits of iris noise without introducing errors due to local variations in the image. All these iterative techniques generally look for to increase the accuracy of iris borders location.

Combined strategies are the result of the combination of different kinds of techniques, performing segmentation in a gradual iris. The aim of these combinations is to increase the accuracy and reduce the computational cost, especially in non-ideal images (either in-distance, on-the-move, no-cooperation environments or dynamic images). That is why these combinations in most of the cases outperform other conventional methods in iris recognition, so much so that three of the eight finalists in the competition NICE.I² are grouped into this category. Table 5 shows the results of the competition finalists NICE.I (2008).

The evaluation of the accuracy in a biometric method of segmentation is a fundamental step, because from here, the final result of matching for recognizing of a person depends on how accurate is this segmentation.

Image capturing on less constrained conditions lead to the appearance of extremely heterogeneous images, with several other types of data in the captured iris regions (e.g., iris obstructions due to eyelids or eyelashes, reflections, off- angle or motion blurred images), it makes the segmentation becomes more difficult. In the competition NICE.I [87], the accuracy of these methods of segmentation were measured, which address several of the above mentioned noises.

Table 5. The NICE.I contest winners using UBIRIS.v2.

Rank	Paper title	Author	Country	Error
1	Efficient and robust segmentation of noisy iris images for non-cooperative iris recognition	Tan et al.	China	0.0131
2	Reliable algorithm for iris segmentation in eye image	Sankowski et al.	Poland	0.0162
3	A knowledge-based approach to the iris segmentation problem	Almeida	Portugal	0.0180
4	Robust and accurate iris segmentation in very noisy iris images	Li et al.	China	0.0224
5	A new iris segmentation method for non-ideal iris images	Jeong et al.	Korea	0.0282

² NICE.I: Noisy Iris Challenge Evaluation - Part I. URL: <http://nice1.di.ubi.pt/>

6	A highly accurate and computationally efficient approach for unconstrained iris segmentation	Chen et al.	USA	0.0297
7	Noisy iris segmentation with boundary regularization and reflections removal	Labati et al.	Italy	0.0301
8	Robust iris segmentation on uncalibrated noisy images using mathematical morphology	Luengo-Oroz et al.	Spain	0.0305

One of the most important problems of the images used for the NICE.I competition is the presence of wide reflections. For this reason, most of the more accurate segmentation methods include a reflection removal step before the actual estimation of the iris boundaries.

In [88], they show results of three iris segmentation techniques. The three selected algorithms were (a) Daugman's integro-differential operator, (b) Hough transform, and finally (c) geodesic active contours. They evaluated segmentation performance on ICE database containing a total of 2,953 iris images corresponding to the left and right eyes. The image quality was quite good, as they were obtained from the cooperative users. However, some images show eyelids or eyelashes occlusions. The performance of an iris segmentation technique was measured by calculating the segmentation accuracy as follows:

$$\text{Segmentation accuracy} = \frac{\text{Number of correctly segmented images}}{\text{Number of input images}} * 100. \quad (34)$$

The Table 6 shows the results of the segmentation of the three techniques. It can be seen that the geodesic active contours provide better performance of segmentation compared with classical approaches. However, it should be noted that the cost of calculating the classical approaches is much less than the geodesic active contours. Therefore, it is necessary to understand the computational demands and operational requirements of an application before hiring a particular iris segmentation algorithm. Further, the outputs of multiple segmentation algorithms may be combined to generate a single hypothesis for the boundaries of the iris.

Table 6. Segmentation accuracies of the three techniques evaluated.[88]

Segmentation technique	Number of input image	Number of correctly segmented images	Segmentation accuracy (%)
Integro-differential operator	2,953	2,597	87.9
Hough transform	2,953	2,632	89.1
Geodesic active contour	2,953	2,699	91.3

Other recent results are reported in [80]. The compared methods are: 1) an algorithm that approximates the iris boundaries as ellipses by using the integro-differential operator proposed in [12], 2) an implementation of the method proposed in [46], 3) the technique described in [24], 4) and the iris segmentation method presented in [80]. The used datasets were the UBIRIS.v2, 500 iris images collected from the FRGC face database [89], 500 iris images collected from the FERET face database [90], and 500 iris images from the ICE-2006 database. Table 7 summarizes the obtained results in terms of accuracy and computational time.

Table 7. Results reported in [80].

Method	Performance	UBIRIS v.2	FRGC	FERET	ICE-2006
Modified Integro-Differential method	Error (%)	13.97	15.10	16.83	2.39
	Time (s)	2.73	2.73	2.73	2.73
Fourier active contour	Error (%)	6.20	8.10	9.96	1.79
	Time (s)	3.90	4.66	4.69	4.41
T. Tan et al.	Error (%)	1.72	4.20	5.02	2.26
	Time (s)	5.08	5.03	5.01	4.80
H. Proenca	Error (%)	1.87	4.33	4.61	2.66
	Time (s)	0.78	0.78	0.78	0.70

Can be observed the method proposed in [80] makes a significant improvement in terms of computational time compared to other methods in the four databases, while in [24] reported better results in the segmentation accuracy.

4.3 Challenges in Iris segmentation

The performance of an iris segmentation algorithm is affected by the image acquisition process [91]. The majority of iris recognition systems require a significant amount of user cooperation during image acquisition to provide good recognition performance. Iris segmentation can be consummated using simple image-processing techniques for an iris image acquired under near-ideal conditions (e.g., good illumination, cooperative subject, un-occluded iris). This is based on the observation that both iris boundaries show significant variation in pixel intensities across their contours (e.g., iris versus the pupil and iris versus the sclera). However, when an iris image is acquired under non-ideal conditions, segmentation becomes a challenging task. Some of the factors that increase iris segmentation challenging are listed below(Fig. 12),[88]:

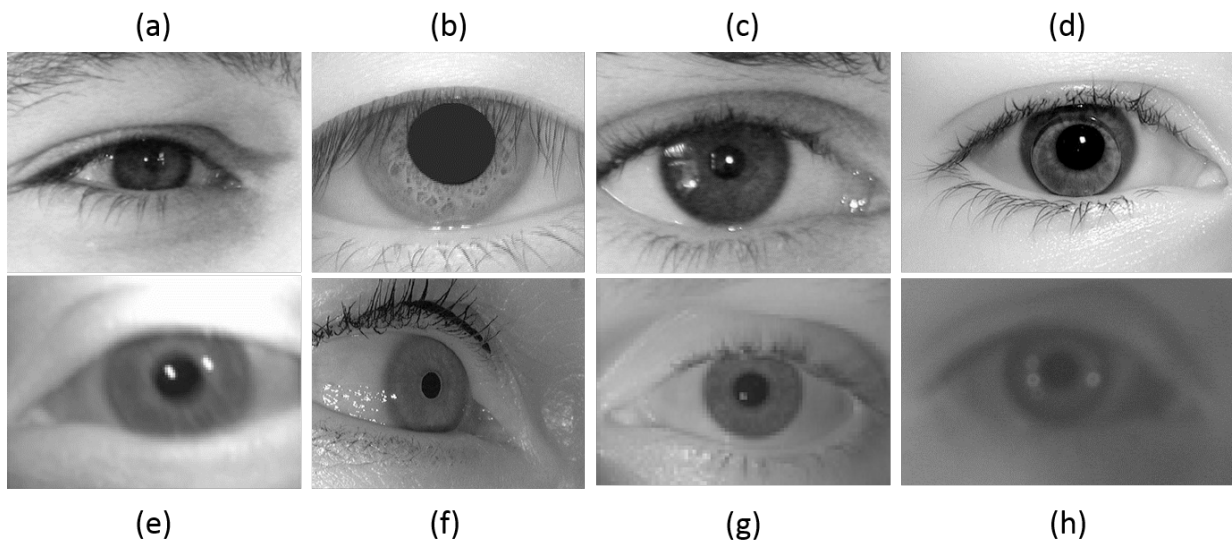


Fig. 11. Examples of iris images showing challenges to be solved in the segmentation. a) Occlusion by eyelids, b) Occlusion by eyelashes, c) Specular reflections, d) Contact lenses, e) Motion blur, f) Off-angle, g) Close-up of an iris image acquired at a large standoff distance, h) Poor illumination.

1. Occlusions caused by the anatomical features of the eye: One of the most common and significant challenge faced during iris segmentation is the occlusion caused by the eyelids and/or the eyelashes.

- **Eyelids:** The eyelids are thin folds of skin that cover and protect the eye from foreign bodies and extreme lighting. The movement of eyelids can be both voluntary (e.g., closing eyelids when tired) and involuntary (e.g., blink caused by a reflex). To obtain an un-occluded image of the iris, the user is required to hold the eyelids wide open for a brief period of time during image acquisition. However, under normal conditions, a minor portion of the human eye is typically occluded on the top and the bottom by the upper and the lower eyelid, respectively. Fig. (11a) shows an iris image exhibiting eyelid occlusion. In such cases, the contour of the limbus boundary is no longer circular or elliptical.

- **Eyelashes:** Eyelashes are the hair at the end of the eyelids. Like eyelids, eyelashes also provide protection to the eye from external fragments. Although the occlusions caused by eyelashes are

minimal, accurate detection of the limbus boundary becomes very difficult in the presence of eyelashes. This is due to the fact that eyelashes can cause coarse interruptions at the limbus boundary. Empirical observations reveal that eyelash occlusion is typically more pronounced in Asian subjects, due to the presence of the epicanthic fold. Fig. (11b) shows an iris image with eyelash occlusions.

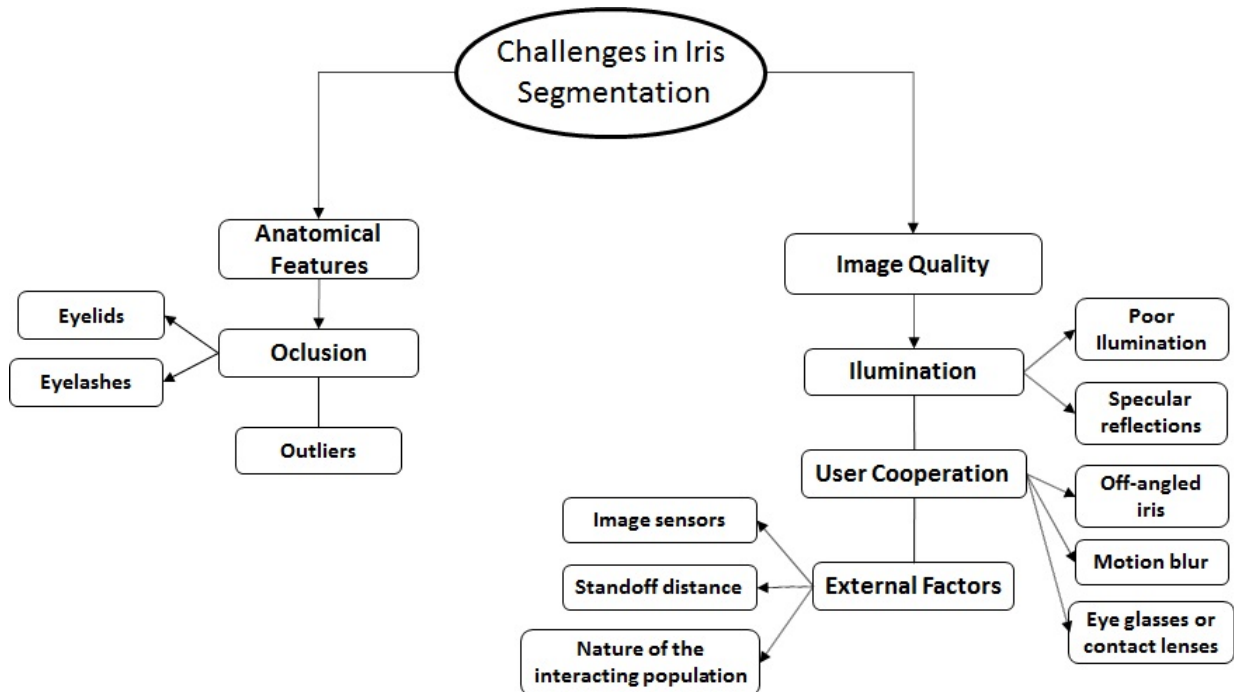


Fig. 12. Challenges in Iris segmentation.

2. **Illumination:** The level and the type of illumination (lighting) used, along with the eye region on which it is focused, play an important role in the quality of an iris image.

- **Poor illumination:** Segmenting an iris image acquired under poor illumination is extremely difficult because the image may offer minimal or no information about the boundaries of the iris. Furthermore, the texture of the iris in such images may not be adequately highlighted, resulting in poor recognition performance. Fig. (11h) shows an iris image acquired under poor illumination conditions.

- **Specular reflections:** Specular reflections are small regions in an iris image characterized by pixels of high-intensity values that are typically caused by improper focusing of the light source. If specular reflections are present on (or even close to) the iris boundaries, iris segmentation becomes difficult. Fig. (11c) shows an iris image with specular reflections on the pupillary boundary.

3. **User cooperation:** Most iris image acquisition systems require a considerable amount of user cooperation to record a good quality image. In cases where the user cooperation is low, the acquired images can be of poor quality, thereby affecting the segmentation performance.

- **Off-angled iris:** Off-angled iris images are caused when the sensor is not orthogonal to the plane of the iris. In such cases, the surface area of the iris is reduced, and the detection of the boundaries becomes difficult. Off-angled iris images are typically caused in situations where the image acquisition is nonideal, i.e., when the subject is in motion or not cognizant of the image acquisition process. Fig. (11f) shows an off-angled iris image.

- **Motion blur:** Motion blur in iris images can occur mainly due to three reasons:

(a) When the image is acquired from a moving subject, (b) movement of the camera, and (c) movement of the subject's eye while adjusting to the device and the environment. In images containing motion blur, the intensity variations across the iris boundaries may be reduced, thereby impacting segmentation. Fig. (11e) shows an image containing motion blur.

- **Eye glasses or contact lenses:** If a user wears an eye glass or contact lens, the acquired iris images may suffer from additional reflection artifacts due to these entities. In a cooperative iris recognition system, this problem can be minimized by requesting the user to avoid wearing eye glasses during image acquisition. However, if a subject wears contact lenses (cosmetic/non-cosmetic), it may not be convenient for the user to remove them, even in a cooperative iris recognition system. Research has shown that contact lenses can impact the performance of iris segmentation and recognition [92]. Fig. (11d) shows the iris image of a user wearing a contact lens (non-cosmetic, hard lens).

4. External factors: Some external factors play a major role in the quality of the input iris images, thereby impacting the segmentation performance.

- **Standoff distance:** Standoff distance refers to the distance of the camera from the subject. If the standoff distance is large, the resolution (number of pixels occupied by the iris region in an image) can be low. In such cases, the iris boundaries may not be clearly distinguishable. Fig. (11g) shows an iris image acquired at a large standoff distance.

- **Image sensors:** The following factors related to image sensors play a significant role in acquiring a good quality iris image:

(a) **Resolution of the sensor:** High-resolution sensors that can capture iris images with a minimum diameter of 200 pixels are preferred over other low-resolution sensors.

(b) **Positioning of the sensor:** The positioning of the sensor plays an important role in acquiring an iris image of good quality. For example, if the iris sensor is placed above or below the eye level of a subject, the acquired image may contain an off-angled iris.

(c) **Sensor noise:** Although not seen as a major factor, sensor noise can produce artifacts in an image, thereby affecting iris segmentation.

- **Nature of the interacting population:** To acquire a good quality iris image, it is required for the target population to be cooperative and habituated with the iris image acquisition system.

- **Outliers:** In very rare cases, abnormalities in the shape of the iris can cause problems with segmentation. In such cases, it can be noticed that the iris boundaries are neither circular nor elliptical.

5 Conclusion

This report has made an analysis of the current state of existing iris segmentation methods. These methods are very important in the process of iris detection from images, since the results quality of the people identification depends on the iris segmentation process. In less controlled environments this task becomes more difficult, for examples, the captured iris image has more noise and blur, the reflections increase, presence of ghosting, the off-angle iris are inevitable, besides occlusions by eyelids, eyelashes among others. Between the proposed techniques in literature, the Daugman's integro-differential operator and Hough transform are the most used; both in test and commercial environments, they estimate the iris borders with two circles. These methods under unrestricted conditions can decrease their accuracy. This is because most of the proposed algorithms in the past assume that the input image of the eye has a good quality. However, there is growing need for faster and more accurate of iris recognition systems, has relaxed the conditions imposed during image acquisition. As a result, image quality can be reduced, forcing the need for robust segmentation algorithms that can tolerate a wide variety of image degradations.

A series of iris segmentation algorithms were discussed in this report. From this discussion, it is clear that (a) iris segmentation is a major problem in the process of iris recognition, (b) a substantial effort has been invested by researchers in solving the problem of iris segmentation under different scenarios: indoor and outdoor: from controlled to uncontrolled conditions; different kind of illumination: from NIR to visible lighting appearing news negative effects; in static and movement conditions, (c) the development of an iris segmentation algorithm depends on a number of image characteristics, such as intrinsic image resolution, degree of iris occlusion, (d) computational demands of different iris segmentation algorithms can vary considerably from one to other real application, and (e) evaluation of the output of an iris segmentation routine and combining the outputs of multiple methods of iris segmentation are ongoing activities in the field of iris biometrics.

References

1. Group, I.B., Biometrics market and industry report 2009-2014. 2011.
2. Daugman, J.G., High confidence visual recognition of persons by a test of statistical independence. *Pattern Analysis and Machine Intelligence*, IEEE Transactions on, 1993. **15**(11): p. 1148-1161.
3. Anil, K.J., B. Ruud, and P. Sharath, Biometrics: personal identification in networked society1999: kluwer academic publishers.
4. Kronfeld, P. and H. Davson, Gross anatomy and embryology of the eye. *The Eye*, 1962. **Academic**.
5. Wolf, E., *The Anatomy of the eye and orbit*. London: H. K. Lewis, 1948.
6. Daouk, C., et al. Iris recognition. in *IEEE ISSPIT*. 2002.
7. Bowyer, K.W., K. Hollingsworth, and P.J. Flynn, Image understanding for iris biometrics: A survey. *Comput. Vis. Image Underst.*, 2008. **110**(2): p. 281-307.
8. ISO/IEC, ISO/IEC-19794-6:2005(E): Information technology - Biometric data interchange formats. Part 6: Iris image data., in Subcommittee SC 37, Biometrics, International Standard Organization, First edition, © ISO/IEC 2005.2005.
9. He, Z., et al., Toward Accurate and Fast Iris Segmentation for Iris Biometrics. *Pattern Analysis and Machine Intelligence*, IEEE Transactions on, 2009. **31**(9): p. 1670-1684.
10. Daugman, J., Iris recognition border-crossing system in the uae. *International Airport Review*, 2004. **8**(2).
11. Li, M., et al., Efficient iris recognition by characterizing key local variations. *Image Processing*, IEEE Transactions on, 2004. **13**(6): p. 739-750.
12. Daugman, J., How iris recognition works. *Circuits and Systems for Video Technology*, IEEE Transactions on, 2002. **14**(1): p. 21-30.
13. Li, Y.-H. and M. Savvides, Iris recognition, overview, in *Encyclopedia of Biometrics2009*, Springer. p. 810-819.
14. Swati, D.S., D.S. Suvarna, and D. Gupta, Article: Iris Recognition. *IJCA Proceedings on Emerging Trends in Computer Science and Information Technology (ETCSIT2012)* etcsit1001, 2012. **ETCSIT**(1): p. 20-23.

15. Ma, L., Y. Wang, and T. Tan. Iris recognition based on multichannel Gabor filtering. in Proc. Fifth Asian Conf. Computer Vision. 2002.
16. Jiali, C., et al. A fast and robust iris localization method based on texture segmentation. in Defense and Security. 2004. International Society for Optics and Photonics.
17. Wildes, R.P., Iris recognition: an emerging biometric technology. *Proceedings of the IEEE*, 1997. **85**(9): p. 1348-1363.
18. Ritter, N. and J. Cooper. Locating the iris: A first step to registration and identification. in Proceedings of 9th IASTED International Conference on Signal and Image Processing. 2003.
19. Mäenpää, T., An Iterative Algorithm for Fast Iris Detection, in *Advances in Biometric Person Authentication*, S. Li, et al., Editors. 2005, Springer Berlin Heidelberg. p. 127-134.
20. Labati, R.D., V. Piuri, and F. Scotti. Neural-based iterative approach for iris detection in iris recognition systems. in *Computational Intelligence for Security and Defense Applications*, 2009. CISDA 2009. IEEE Symposium on. 2009.
21. Mohammadi, A.E. A study of segmentation and normalization for iris recognition systems. in Thesis requirement for the degree of Master of Applied Science in Systems Design Engineering. 2006. Waterloo, Ontario, Canada
22. Sreecholpech, C. and S. Thainimit. A robust model-based iris segmentation. in *Intelligent Signal Processing and Communication Systems*, 2009. ISPACS 2009. International Symposium on. 2009.
23. Boles, W.W. and B. Boashash, A human identification technique using images of the iris and wavelet transform. *Signal Processing, IEEE Transactions on*, 1998. **46**(4): p. 1185-1188.
24. Tieniu, T., H. Zhaofeng, and S. Zhenan, Efficient and robust segmentation of noisy iris images for non-cooperative iris recognition. *Image and Vision Computing*, 2010. **28**(2): p. 223-230.
25. Labati, R.D. and F. Scotti, Noisy iris segmentation with boundary regularization and reflections removal. *Image and Vision Computing*, 2010. **28**(2): p. 270-277.
26. Li, P., et al., Robust and accurate iris segmentation in very noisy iris images. *Image and Vision Computing*, 2010. **28**(2): p. 246-253.
27. Bastos, C.A.C.M., I.R. Tsang, and G.D.C. Calvalcanti. A combined Pulling & Pushing and Active Contour method for pupil segmentation. in *Acoustics Speech and Signal Processing (ICASSP)*, 2010 IEEE International Conference on. 2010.
28. Zhi-yong, P., L. Hong-zhou, and L. Jian-ming, An Improvement Method for Daugman's Iris Localization Algorithm, in *Advances in Neural Networks – ISNN 2011*, D. Liu, et al., Editors. 2011, Springer Berlin Heidelberg. p. 364-372.
29. Shamsi, M., et al. Fast Algorithm for Iris Localization Using Daugman Circular Integro Differential Operator. in *Soft Computing and Pattern Recognition*, 2009. SOCPAR '09. International Conference of. 2009.
30. Wojciech, S., et al., Reliable algorithm for iris segmentation in eye image. *Image and Vision Computing*, 2010. **28**(2): p. 231-237.
31. Xinying, R., et al., An improved method for Daugman's iris localization algorithm. *Computers in Biology and Medicine*, 2008. **38**(1): p. 111-115.
32. Kashima, H., et al., An Iris Detection Method Using the Hough Transform., in *The 5th Asian Conference on Computer Vision.2002: Melbourne, Australia*. p. 23-25.
33. Noureddine, C., C.F. Zohra, and D. Amar, Circular Hough Transform for Iris localization. *Science and Technology*, 2012. **2**(5): p. 114-121.
34. Xu, Z. and P. Shi. A Robust and Accurate Method for Pupil Features Extra. in *18th International Conference on Pattern Recognition (ICPR'06) 2006*. ICPR.
35. Proenca, H. and L.A. Alexandre, Iris segmentation methodology for non-cooperative recognition. *Vision, Image and Signal Processing, IEE Proceedings -*, 2006. **153**(2): p. 199-205.
36. Masek, L., Recognition of human iris patterns for biometric identification, 2003, Master's thesis, University of Western Australia.
37. Xinhua, F., et al. Iris Localization with Dual Coarse-to-fine Strategy. in *Pattern Recognition*, 2006. ICPR 2006. 18th International Conference on. 2006.
38. Tian, Q.-C., et al. Fast algorithm and application of Hough transform in iris segmentation. in *Machine Learning and Cybernetics*, 2004. Proceedings of 2004 International Conference on. 2004.
39. Sundaram, R.M., B.C. Dhara, and B. Chanda. A Fast Method for Iris Localization. in *Emerging Applications of Information Technology (EAIT)*, 2011 Second International Conference on. 2011.

40. Martin-Roche, D.D., C. Sanchez-Avila, and R. Sanchez-Reillo. Iris recognition for biometric identification using dyadic wavelet transform zero-crossing. in *Security Technology, 2001 IEEE 35th International Carnahan Conference on*. 2001.
41. Puhan, N.B., N. Sudha, and J. Xudong. Robust eyeball segmentation in noisy iris images using fourier spectral density. in *Information, Communications & Signal Processing, 2007 6th International Conference on*. 2007.
42. Chan, T.F. and L.A. Vese, Active contours without edges. *Image Processing, IEEE Transactions on*, 2001. **10**(2): p. 266-277.
43. Zhang, X., Z. Sun, and T. Tan. Texture removal for adaptive level set based iris segmentation. in *Image Processing (ICIP), 2010 17th IEEE International Conference on*. 2010.
44. Vatsa, M., R. Singh, and A. Noore, Improving iris recognition performance using segmentation, quality enhancement, match score fusion, and indexing. *IEEE Trans Syst Man Cybern B Cybern*, 2008. **38**(4): p. 1021-35.
45. Shah, S. and A. Ross, Iris Segmentation Using Geodesic Active Contours. *Information Forensics and Security, IEEE Transactions on*, 2009. **4**(4): p. 824-836.
46. Daugman, J., *New Methods in Iris Recognition. Systems, Man, and Cybernetics, Part B: Cybernetics*, IEEE Transactions on, 2007. **37**(5): p. 1167-1175.
47. Freund, Y. and R.E. Schapire. A decision-theoretic generalization of on-line learning and an application to boosting. in *Computational learning theory*. 1995. Springer.
48. Viola, P. and J. M. Rapid object detection using a boosted cascade of simple features. in *Computer Vision and Pattern Recognition, 2001. CVPR 2001. Proceedings of the 2001 IEEE Computer Society Conference on*. 2001.
49. He, Z., T. Tan, and Z. Sun. Iris Localization via Pulling and Pushing. in *Pattern Recognition, 2006. ICPR 2006. 18th International Conference on*. 2006.
50. Jinyu, Z. and N.A. Schmid, On a Methodology for Robust Segmentation of Nonideal Iris Images. *Systems, Man, and Cybernetics, Part B: Cybernetics, IEEE Transactions on*, 2010. **40**(3): p. 703-718.
51. Rongnian, T. and W. Shaojie. Improving Iris Segmentation Performance Via Borders Recognition. in *Intelligent Computation Technology and Automation (ICICTA), 2011 International Conference on*. 2011.
52. Labati, R.D., V. Piuri, and F. Scotti. Agent-based image iris segmentation and multiple views boundary refining. in *Biometrics: Theory, Applications, and Systems, 2009. BTAS '09. IEEE 3rd International Conference on*. 2009a.
53. Sung, H., et al. Iris recognition using collarete boundary localization. in *Pattern Recognition, 2004. ICPR 2004. Proceedings of the 17th International Conference on*. 2004.
54. Lee, K., et al., Efficient Iris Recognition through Improvement of Feature Vector and Classifier. *ETRI Journal*, 2001. **23**: p. 61-70.
55. Luengo-Oroz, M.A. and E. Faure, Robust iris segmentation on uncalibrated noisy images using mathematical morphology. *Image Vision Comput.*, 2010. **28**(2): p. 278-284.
56. Chin, T.C. and E.H. Tat. An efficient one-dimensional fractal analysis for iris recognition. in *Proceedings of the 13-th WSCG International Conference in Central Europe on Computer Graphics, Visualization and Computer Vision*. 2005.
57. Grabowski, K., et al. Reliable Iris Localization Method With Application To Iris Recognition In Near Infrared Light. in *Mixed Design of Integrated Circuits and System, 2006. MIXDES 2006. Proceedings of the International Conference*. 2006.
58. Chia-Te, C., et al., Non-orthogonal view iris recognition system. *Circuits and Systems for Video Technology, IEEE Transactions on*, 2010. **20**(3): p. 417-430.
59. Fitzgibbon, A., M. Pilu, and R.B. Fisher, Direct least square fitting of ellipses. *Pattern Analysis and Machine Intelligence, IEEE Transactions on*, 1999. **21**(5): p. 476-480.
60. Chen, Y., S.C. Dass, and A.K. Jain, Localized iris image quality using 2-d wavelets, in *Proceedings of the 2006 international conference on Advances in Biometrics2006*, Springer-Verlag: Hong Kong, China. p. 373-381.
61. Kong, W.K. and D. Zhang. Accurate iris segmentation based on novel reflection and eyelash detection model. in *Intelligent Multimedia, Video and Speech Processing, 2001. Proceedings of 2001 International Symposium on*. 2001.
62. Huang, J., et al. A new iris segmentation method for recognition. in *Pattern Recognition, 2004. ICPR 2004. Proceedings of the 17th International Conference on*. 2004.

63. Sik, J.D., et al., A new iris segmentation method for non-ideal iris images. *Image and Vision Computing*, 2010. **28**(2): p. 254-260.
64. Xu, G., Z. Zhang, and Y. Ma. Improving the Performance of Iris Recognition System Using Eyelids and Eyelashes Detection and Iris Image Enhancement. in *Cognitive Informatics, 2006. ICCI 2006. 5th IEEE International Conference on*. 2006.
65. Youbo, Y. and M. Xie. Eyelid and eyelash detection method based on morphology. in *Computer and Automation Engineering (ICCAE), 2010 The 2nd International Conference on*. 2010.
66. Alonso-Fernandez, F. and J. Bigun. Quality factors affecting iris segmentation and matching. in *Biometrics (ICB), 2013 International Conference on*. 2013.
67. Byung Jun, K. and P. Kang Ryoung, Real-Time Image Restoration for Iris Recognition Systems. *Systems, Man, and Cybernetics, Part B: Cybernetics, IEEE Transactions on*, 2007. **37**(6): p. 1555-1566.
68. Zhuoshi, W., et al. Counterfeit iris detection based on texture analysis. in *Pattern Recognition, 2008. ICPR 2008. 19th International Conference on*. 2008.
69. Lim, E., J. Xudong, and Y. WeiYun. Fingerprint quality and validity analysis. in *Image Processing. 2002. Proceedings. 2002 International Conference on*. 2002.
70. Dozier, G.V., et al., Iris Template Extraction Via Bit Inconsistency and GRIT, in *Encyclopedia of Biometrics2009*, Springer. p. 859-865.
71. Jain, A.K., P.J. Flynn, and A.A. Ross, *Handbook of biometrics2008*: Springer.
72. Rathgeb, C., A. Uhl, and P. Wild, *Iris Biometrics: From Segmentation to Template Security2013*: Springer.
73. NIST. NIST: Iris Challenge Evaluation. 2005-2006 [cited 2012; Available from: <http://www.nist.gov/itl/iad/ig/ice.cfm>].
74. MMU:MMU1 and MMU2 Iris Databases. [cited 2012; Available from: <http://pesona.mmu.edu.my/~ccteo/>].
75. Computer Vision Research Laboratory: CVRL Data Sets. [cited 2012; Available from: <http://www.nd.edu/~cvrl/CVRL/DataSets.html>].
76. Flynn, K.W.B.a.P.J., *The ND-IRIS-0405 Iris Image Database*. . 2005.
77. SOCIA Lab, University of Beira Interior. [cited 2012; Available from: <http://iris.di.ubi.pt>].
78. SOCIA Lab, University of Beira Interior: UBIRIS.v1 Database. [cited 2012; Available from: <http://iris.di.ubi.pt/ubiris1.html>].
79. SOCIA Lab, University of Beira Interior: UBIRIS.v2 Database. [cited 2012; Available from: <http://iris.di.ubi.pt/ubiris2.html>].
80. Proenca, H., Iris recognition: On the segmentation of degraded images acquired in the visible wavelength. *Pattern Analysis and Machine Intelligence, IEEE Transactions on*, 2010. **32**(8): p. 1502-1516.
81. Center for Identification Technology Research, West Virginia University: Biometric Dataset Collection. [cited 2012; Available from: <http://www.citer.wvu.edu/biometricdatasetcollections>].
82. Center for Identification Technology Research, West Virginia University: Biometric Dataset Collection. [cited 2012; Available from: http://www.citer.wvu.edu/off_axis_angle_iris_dataset_collection_release1].
83. Bath, U.o. Bath Iris Image Database. [cited Retrieved Aug 2013; Available from: <http://www.smartsensors.co.uk/products/iris-database/>].
84. Palacky University of Olomouc: Iris Database. [cited 2012; Available from: <http://phoenix.inf.upol.cz/iris/>].
85. Indian Institute of Technology Delhi: IIT Delhi Iris Database. [cited 2012; Available from: http://www4.comp.polyu.edu.hk/~csajaykr/IITD/Database_Iris.htm].
86. NIST: Multiple Biometric Grand Challenge. [cited 2012; Available from: <http://www.nist.gov/itl/iad/ig/mbgc.cfm>].
87. Proenca, H. and L.A. Alexandre. The NICE.I: Noisy Iris Challenge Evaluation - Part I. in *Biometrics: Theory, Applications, and Systems, 2007. BTAS 2007. First IEEE International Conference on*. 2007.
88. Jillela, R. and A.A. Ross, Methods for iris segmentation, in *Handbook of Iris Recognition2013*, Springer. p. 239-279.
89. Phillips, P.J., et al. Overview of the face recognition grand challenge. in *Computer vision and pattern recognition, 2005. CVPR 2005. IEEE computer society conference on*. 2005. IEEE.
90. Phillips, P.J., et al., The FERET evaluation methodology for face-recognition algorithms. *Pattern Analysis and Machine Intelligence, IEEE Transactions on*, 2000. **22**(10): p. 1090-1104.
91. Zuo, J., K.N. D, and S.N. A. A robust iris segmentation procedure for unconstrained subject presentation. in *Biometric Consortium Conference, 2006 Biometrics Symposium: Special Session on Research at the*. 2006. IEEE.
92. Baker, S., et al., Degradation of iris recognition performance due to non-cosmetic prescription contact lenses. *Computer Vision and Image Understanding*, 2010. **114**(9): p. 1030-1044.

RT_059, enero 2014

Aprobado por el Consejo Científico CENATAV

Derechos Reservados © CENATAV 2014

Editor: Lic. Lucía González Bayona

Diseño de Portada: Di. Alejandro Pérez Abraham

RNPS No. 2142

ISSN 2072-6287

Indicaciones para los Autores:

Seguir la plantilla que aparece en www.cenatav.co.cu

C E N A T A V

7ma. A No. 21406 e/214 y 216, Rpto. Siboney, Playa;

La Habana. Cuba. C.P. 12200

Impreso en Cuba

